Research Square

Preprints are preliminary reports that have not undergone peer review.
They should not be considered conclusive, used to inform clinical practice,
or referenced by the media as validated information.

Analytical Characterization and Design Guidelines for Membrane Permeation Based on a Four-State Master Equation

Ikuo Fukuda

ifukuda@omu.ac.jp

Osaka Metropolitan University

Kazuma Fukui

Osaka Metropolitan University

Yoshiki Miyazawa

Chugai Pharmaceutical Co. Ltd.

Hironori Kokubo

Chugai Pharmaceutical Co. Ltd.

Kei Moritsugu

Osaka Metropolitan University

Research Article

Keywords:

Posted Date: November 23rd, 2026

DOI: https://doi.org/10.21203/rs.3.rs-11815739/v1

License: This work is licensed under a Creative Commons Attribution 4.0 International License.
Read Full License

Additional Declarations: No competing interests reported.

Analytical Characterization and Design Guidelines for Membrane Permeation Based on a Four-State Master Equation

Ikuo Fukuda*[1,2], Kazuma Fukui[1], Yoshiki Miyazawa[3], Hironori Kokubo[3], and Kei Moritsugu[1,2]

[1*] *Graduate School of Science, Osaka Metropolitan University, 1-2 Gakuen-cho, Naka-ku, Sakai, Osaka 599-8570, Japan*

[2] *Graduate School of Drug Discovery Sciences, Osaka Metropolitan University, 1-2 Gakuen-cho, Naka-ku, Sakai, Osaka 599-8570, Japan and*

[3] *Chugai Pharmaceutical Co. Ltd., Yokohama, Kanagawa 244-8602,Japan*

(Dated: November 20, 2026)

Abstract

Membrane permeation of molecules is important in drug discovery and molecular transport, where the permeation rate is a key determinant of performance. In this study, we combine mathematical analysis based on the master equation with molecular simulations to investigate the passive permeation of molecules across membranes. Through an analysis of a four-state master equation, we derive explicit expressions for the eigenvalues and establish conditions under which the eigenvalue with the smallest absolute value can be regarded as characterizing membrane permeation. We also derive conditions under which the permeation rate can be approximated using a single rate parameter obtained from molecular simulations, and verify these findings for four small molecules. These results provide an explicit link between kinetic parameters and macroscopic transport properties, offering a theoretical framework for interpreting simulation data and guiding molecular design.

* Author to whom correspondence should be addressed: ifukuda@omu.ac.jp

I. INTRODUCTION

Membrane permeation of various molecules is of great importance in fields such as drug discovery, pharmacokinetic evaluation, and nanomaterial design [1, 2]. In particular, passive molecular transport across cell membranes and lipid bilayers is closely related to the mechanisms underlying drug efficacy and toxicity. Therefore, quantitatively understanding the permeation rate and permeation amount is an important practical issue. A better understanding of membrane permeation can also contribute to the development of molecular design guidelines and highly efficient transport systems.

In recent years, molecular simulations, including molecular dynamics (MD) simulations [3, 4], have been widely used to investigate membrane permeation phenomena [5–8]. Detailed molecular-level mechanisms have been investigated through calculations of free-energy profiles and analyses of permeation pathways [9–13]. In addition, methods such as the Markov State Model (MSM) [14] and the weighted ensemble (WE) method [15] have been employed to statistically extract transition probabilities and dynamical information.

However, membrane permeation generally occurs on time scales of microsecond or longer [8], making direct molecular simulations computationally demanding. To address this problem, various methods have been developed to efficiently describe long-time dynamics. One effective approach is to combine molecular simulations with master equations. For example, Dickson *et al.* [16] combined the MSM [17] with a master equation to evaluate membrane permeability with higher accuracy than conventional approaches, while Ghaemi *et al.* [18] describe a method to derive a master equation from the analysis of MD simulations. Furthermore, combining molecular simulations with umbrella sampling [19] or milestoning theory [20] enables efficient sampling of rare events.

The master equation has been widely used as a theoretical framework for describing physicochemical processes [21]. In particular, the chemical master equation [22] provides a fundamental description of dynamics in chemical reaction networks and molecular transport processes. Various approaches to analyzing the chemical master equation have been developed, including the finite state projection method [23], analytical solutions for specific classes of reaction systems [24], and stochastic approximations such as the chemical Fokker–Planck equation [25]. Comprehensive reviews have also covered approximation methods and parameter inference in stochastic biochemical kinetics [26]. Nevertheless, explicit analyti-

cal relationships between kinetic rate parameters and macroscopic observables, particularly under general initial conditions, remain insufficiently understood.

In this study, we focus on a four-state linear master equation as a minimal model for membrane permeation by passive diffusion and analyze its spectral structure. The four states correspond to physically natural regions: the exterior of the membrane (extracellular region), the first and second lipid phases within the membrane, and the exterior of the membrane on the opposite side (intracellular region). The transitions of the states are characterized by three rate parameters, k_{in}, k_{out}, and k_{tra}. In previous studies combining master equations with molecular simulations, solutions of the equations have commonly been obtained numerically, or asymptotic behavior has been characterized through empirical fitting [16, 27]. In contrast, we analytically derive the eigenvalues and eigenvectors of the transition matrix and express the time scale governing permeation and its parameter dependence in explicit functional forms. Thus, the transport properties can be directly related to the rate parameters. Although spectral analysis generally becomes rapidly more complicated for higher-dimensional systems, the four-state system considered here is constructed as a minimal model that combines physical plausibility with analytical tractability.

In this study, we focus primarily on the permeation rate as a characteristic measure of the permeation process. First, for the permeation rate, we show that the eigenvalue with the smallest absolute value among the nonzero eigenvalues of the transition matrix, for which we denote this eigenvalue by C hereafter, can determine the time scale of permeation. To this end, we first analyze the modes under a typical initial condition and then under general initial conditions, and examine the properties of C. We find that, in general, C, or the corresponding eigenmode, does not necessarily provide the best description of the permeation process. On the other hand, we derive a simple condition that holds over a practically sufficiently broad parameter region and under which C characterizes permeation. This establishes, under explicit mathematical conditions, the correspondence between C and the permeation rate. As a result, the permeation rate can be calculated from the three rate parameters on a theoretical basis. We also define the permeation amount as a measure based on the probability of eventually reaching state 4 and analyze its parameter dependence.

Furthermore, we analyze in detail the dependence of C on the rate parameters $(k_{in}, k_{out}, k_{tra})$. We find that the permeation rate increases with increasing k_{in} and k_{tra}, whereas it decreases with increasing k_{out}. In addition, we mathematically show that, in a

specific parameter region, the permeation rate can be approximated by the simple expression $2k_{tra}$, indicating that it is effectively governed only by k_{tra}, which characterizes the transition rate within the membrane. These results simplify the evaluation of the permeation rate and provide guidelines for identifying which process should be controlled in molecular design.

In this study, we apply the weighted ensemble (WE) simulation method by Zuckerman and co-workers [28, 29] to the calculation of the rate parameters in the master equation. In WE simulations, a large number of short molecular dynamics (MD) simulations are run to generate a diverse set of continuous trajectories. Each trajectory is assigned a statistical weight, and the sum of the weights is used to compute the population dynamics. The extracted rate parameter were used to validate the theoretical analysis by confirming the derived conditions. Although the rate parameters obtained here pertain to small molecules, understanding small-molecule permeation provides a foundation for investigating the permeation of larger and more polar molecules, including compounds beyond the Rule of Five and cyclic peptides, a middle-sized modality [30, 31].

The remainder of this paper is organized as follows. Section II presents the formulation of the four-state master equation and its spectral analysis. Section III considers the time evolution of the master equation for a typical initial condition in which particles are initially localized in state 1, and analyzes the time evolution of each decomposed mode. Section IV considers more general initial conditions and analyze sign patterns of the mode-expansion coefficients. Section V clarifies the conditions on the initial values that need to be considered. Section VI derives the conditions under which C characterizes the permeation process. Section VII examines the dependence of the C on the rate parameters. We further derive the conditions under which it can be approximated by $2k_{tra}$. Section VIII presents molecular simulations of membrane permeation using the WE method and validates the theoretical analysis. Section IX discusses the characteristics of the master equation approach and the permeation amount, including its relationship with the permeation rate. Finally, Section X presents the conclusions and future perspectives.

II. FOUR-STATE LINEAR MODEL

A. Model Definition

The passive permeation of target molecules across a membrane can be modeled as a diffusion process. Fick's law, which states that the diffusive flux is proportional to the concentration gradient, describes diffusion in a uniform environment. Molecular permeation across a membrane, however, is affected by a heterogeneous environment. In particular, local changes in the dynamics, such as the entry of molecules from the aqueous phase into the membrane (interfacial barriers) and the retention of highly lipophilic molecules within the membrane (trapping), can play essential roles. This heterogeneity can be represented by a potential function, and a master equation can be derived from the Smoluchowski equation, which incorporates this effect into the Fickian flux [32].

In the four-state master equation model, the system is divided into four sites: the aqueous phase outside the membrane (extracellular region), the first and second distinct lipid phases within the membrane, and the aqueous phase outside the membrane on the opposite side (intracellular region). The state of each site is represented by the probability of finding a target molecule at that site, or equivalently by a normalized molecular population, p_1, p_2, p_3, p_4. The probabilities of the four states evolve through molecular exchange between neighboring states, as illustrated in Fig. 1. The exchange is characterized by the rate parameters k, and the resulting transition rates are assumed to depend linearly on the state probabilities. The resulting transitions, namely, the time evolution of $\mathbf{p} = (p_1, p_2, p_3, p_4)$, are described by the following four-state master equation, which is a system of linear ordinary differential equations:

$$\frac{d\mathbf{p}}{dt} = K\mathbf{p}. \tag{1}$$

Here, the positive rate parameters $k_{in}, k_{out}, k_{tra} > 0$ define the transition matrix

$$K = \begin{pmatrix} -k_{in} & k_{out} & 0 & 0 \\ k_{in} & -(k_{out} + k_{tra}) & k_{tra} & 0 \\ 0 & k_{tra} & -(k_{tra} + k_{out}) & k_{in} \\ 0 & 0 & k_{out} & -k_{in} \end{pmatrix}. \tag{2}$$

This matrix satisfies probability conservation (or particle-number conservation), since the sum of the elements in each column is zero. The transitions between states 1 and 2 and

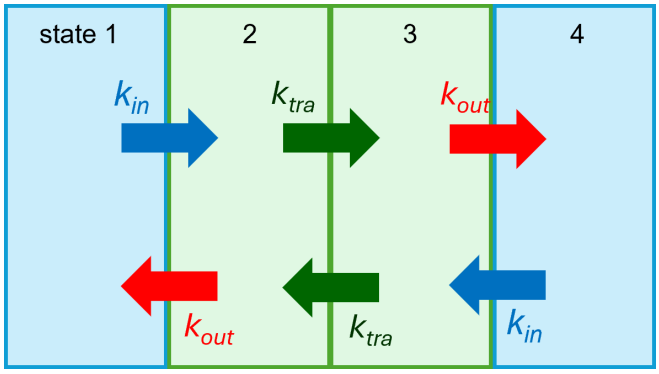


FIG. 1: The system is divided into four sites: (site 1) the aqueous phase outside the membrane (extracellular region), (site 2) the first lipid phase and (site 3) second distinct lipid phase within the membrane, and (site 4) the aqueous phase outside the membrane on the opposite side (intracellular region). State i, state of site i, is represented by the probability of finding a target molecule at that site, p_i, for $i = 1, .., 4$. These probabilities evolve through molecular exchange between neighboring states characterized by the rate parameters k_{in}, k_{out}, and k_{tra}.

between states 3 and 4 are characterized by the rate parameters k_{in} and k_{out}, while the forward and backward rates between states 2 and 3 are both equal to k_{tra}.

In the present model, the individual transition processes can be described by distinct rate parameters k_{in}, k_{out}, k_{tra} without assuming a spatially uniform macroscopic diffusion coefficient. This allows local differences in the environment associated with membrane permeation, such as interfacial barriers and molecular retention within the membrane, to be incorporated into the respective transition processes.

B. Eigenvalues

The eigenvalues λ of the transition matrix K are obtained as solutions to the characteristic equation $\det(K - \lambda I) = 0$. The three nonzero eigenvalues, other than $\lambda_0 = 0$, which correspond to the steady state, are as follows:

$$A = -(k_{in} + k_{out}), \tag{3a}$$

$$B = \frac{1}{2}\left(-(k_{in} + k_{out} + 2k_{tra}) - \sqrt{D}\right), \tag{3b}$$

$$C = \frac{1}{2}\left(-(k_{in} + k_{out} + 2k_{tra}) + \sqrt{D}\right), \tag{3c}$$

where

$$D = (k_{in} + k_{out} + 2k_{tra})^2 - 8k_{in}k_{tra}. \tag{4}$$

The following relationships always hold for these eigenvalues (the proof is given in Appendix A):

$$B < A < C < 0. \tag{5}$$

Therefore, there is no degeneracy of eigenvalues, and all eigenvalues other than zero are negative (relaxation modes). In this 4-state model, the minimum absolute value of the nonzero eigenvalues corresponds (excluding the proportionality factor) to the permeation rate. This interpretation is discussed in detail in Sec. VI, and its relation to the permeation coefficient is made explicit in Sec. VIII C.

C. Time development of the solutions

The solution of the master equation (1) with an initial value $\mathbf{p}(0) \in \mathbb{R}^4$ is

$$t \mapsto \mathbf{p}(t) \equiv (p_1(t), p_2(t), p_3(t), p_4(t)) = \exp(tK)\mathbf{p}(0). \tag{6}$$

In order for each $p_i(t)$ to be interpreted as a probability associated with site i, it is necessary for $\mathbf{p}(t)$ to be a probability vector—that is, to belong to a subset

$$\textstyle\sum^4 \equiv \left\{ \mathbf{p} \in \mathbb{R}^4 \mid p_1, p_2, p_3, p_4 \geq 0,\ \sum_{i=1}^4 p_i = 1 \right\}. \tag{7}$$

It follows that

$$\forall t \geq 0,\ \mathbf{p}(t) \in \textstyle\sum^4 \tag{8}$$

for $\mathbf{p}(0) \in \sum^4$ from the properties of the matrix K such that $\sum_{i=1}^4 K_{ij} = 0$ for any j and that $K_{ij} \geq 0$ for any $i \neq j$.

The solution (6) can also be expressed as a linear combination of eigenmodes (the time evolution along the direction of each eigenvector) such that

$$\mathbf{p}(t) = c_0\mathbf{v}_0 + c_A\mathbf{v}_A e^{At} + c_B\mathbf{v}_B e^{Bt} + c_C\mathbf{v}_C e^{Ct}. \tag{9}$$

Although these two equations are equivalent, Eq. (9) is easier to interpret physically, so we will examine it below.

D. Eigenvectors and Expansion Coefficients

Eigenvectors corresponding to eigenvalues $\lambda = 0, A, B, C$, respectively, are

$$\mathbf{v}_0 = \begin{pmatrix} k_{out} \\ k_{in} \\ k_{in} \\ k_{out} \end{pmatrix}, \ \mathbf{v}_A = \begin{pmatrix} 1 \\ -1 \\ -1 \\ 1 \end{pmatrix}, \ \mathbf{v}_B = \begin{pmatrix} -1 \\ -\alpha \\ \alpha \\ 1 \end{pmatrix}, \quad \mathbf{v}_C = \begin{pmatrix} -1 \\ -\beta \\ \beta \\ 1 \end{pmatrix}. \tag{10}$$

Since there is no degeneracy, these are uniquely determined up to a constant multiple, and $\{\mathbf{v}_0, \mathbf{v}_A, \mathbf{v}_B, \mathbf{v}_C\}$ form a linear basis for $\mathbb{R}^4$. Here, α and β, appeared in the components of $\mathbf{v}_B$ and $\mathbf{v}_C$, are defined by

$$\alpha = \frac{k_{in} - k_{out} - 2k_{tra} - \sqrt{D}}{2k_{out}}, \tag{11a}$$

$$\beta = \frac{k_{in} - k_{out} - 2k_{tra} + \sqrt{D}}{2k_{out}}. \tag{11b}$$

It can be shown that α and β have definite signs such as

$$\alpha < 0, \tag{12a}$$

$$\beta > 0, \tag{12b}$$

which can be shown using Eq. (97) in Appendix D. These signs are important for understanding the time development of the eigenmodes discussed in Sec. III.

The expansion coefficients in Eq. (9) is determined by

$$\begin{pmatrix} c_0 \\ c_A \\ c_B \\ c_C \end{pmatrix} = V^{-1}\mathbf{p}(0), \tag{13}$$

where V^{-1} is the inverse matrix of

$$V := [\mathbf{v}_0, \mathbf{v}_A, \mathbf{v}_B, \mathbf{v}_C] \in \mathrm{GL}(4; \mathbb{R}). \tag{14}$$

III. TIME EVOLUTION FOR $\mathbf{p}(0) = (1, 0, 0, 0)^{\mathrm{T}}$

From a physicochemical perspective, the case

$$\mathbf{p}(0) = (1, 0, 0, 0)^{\mathrm{T}} \tag{15}$$

is of particular interest, in which particles are initially localized in state 1. For example, this initial condition was considered in the theoretical study by Dickson *et al.* [16] and in the experimental setup of the PAMPA assay for cyclic peptides by Furukawa *et al.* [33]. More general initial conditions are discussed in Sec. IV.

In Sec. III A, we derive explicit expressions for the expansion coefficients in Eq. (13) for the initial condition given by Eq. (15). In Sec. III B, we examine the time evolution of each mode and discuss its physical interpretation. In Sec. III C, we examine the time evolution of state 4.

A. Expansion coefficients and their definite signs

By substituting Eq. (10) into Eq. (14) to find the inverse matrix, and then applying it to Eq. (13) with Eq. (15), we obtain the following results (as the first column of V^{-1}):

$$c_0 = \frac{1}{2(k_{in} + k_{out})} > 0, \tag{16a}$$

$$c_A = \frac{k_{in}}{2(k_{in} + k_{out})} > 0, \tag{16b}$$

$$c_B = \frac{-2k_{out}\beta}{4\sqrt{D}} = -\frac{\beta}{2(\beta - \alpha)} < 0, \tag{16c}$$

$$c_C = \frac{2k_{out}\alpha}{4\sqrt{D}} = \frac{\alpha}{2(\beta - \alpha)} < 0. \tag{16d}$$

where the signs of c_0 and c_A are clearly obtained and those of c_B and c_C are obtained by Eq. (12a)–(12b).

B. Time Evolution and Physical Interpretation of Each Mode

To examine the specific time evolution of $\mathbf{p}(t)$, substitute Eq. (16) into Eq. (9), and, taking into account the signs of each quantity, we obtain

$$\begin{aligned}\mathbf{p}(t) &= c_0\mathbf{v}_0 + c_A\mathbf{v}_A e^{-|A|t} + c_B\mathbf{v}_B e^{-|B|t} + c_C\mathbf{v}_C e^{-|C|t} \\ &= |c_0| \begin{pmatrix} k_{out} \\ k_{in} \\ k_{in} \\ k_{out} \end{pmatrix} + |c_A| e^{-|A|t} \begin{pmatrix} 1 \\ -1 \\ -1 \\ 1 \end{pmatrix} + |c_B| e^{-|B|t} \begin{pmatrix} 1 \\ -|\alpha| \\ |\alpha| \\ -1 \end{pmatrix} + |c_C| e^{-|C|t} \begin{pmatrix} 1 \\ |\beta| \\ -|\beta| \\ -1 \end{pmatrix}. \end{aligned} \tag{17}$$

1. Physical Interpretation of Mode C

For mode C, namely,

$$\begin{aligned}\mathbf{p}_C(t) &:= c_C \mathbf{v}_C e^{-|C|t} \\ &= |c_C| e^{-|C|t} \begin{pmatrix} 1 \\ |\beta| \\ -|\beta| \\ -1 \end{pmatrix}, \end{aligned} \tag{18}$$

the first and second components decrease monotonically with respect to time according to

$$t \mapsto \begin{pmatrix} |c_C| e^{-|C|t} \\ |\beta c_C| e^{-|C|t} \end{pmatrix},$$

whereas the third and fourth components increase monotonically according to

$$t \mapsto \begin{pmatrix} -|\beta c_C| e^{-|C|t} \\ -|c_C| e^{-|C|t} \end{pmatrix}.$$

Equivalently, the first and second components of the time derivative of mode C,

$$\mathrm{D}\mathbf{p}_C(t) = -|C||c_C| e^{-|C|t} \begin{pmatrix} 1 \\ |\beta| \\ -|\beta| \\ -1 \end{pmatrix}, \tag{19}$$

are always negative, whereas the third and fourth components are always positive. Thus, the sign pattern of mode C is always $(-,-,+,+)$, so that the probabilities of states 1 and 2 always decrease, while those of states 3 and 4 always increase. This represents a process in which particles flow from states 1 and 2 to state 3 and then permeate into state 4. This is one reason why the eigenvalue C, or the corresponding eigenmode $\mathbf{p}_C$, can be interpreted physically as a "permeation mode."

The second reason is that, at sufficiently large t, the behavior of $\mathbf{p}(t)$ is dominated by the time evolution associated with C having the smallest absolute value (Eq. (5)), namely, by $\mathbf{p}_C(t)$. This point will be revisited in Sec. III C.

The third reason is that mode C (Eq. (18)) is described using all three parameters k_{in}, k_{out}, and k_{tra}. In other words, this mode is determined by information on all three processes: influx, transport, and efflux. This property does not hold for mode A, as discussed below.

2. Physical Interpretation of the Other Modes

For mode A, namely,

$$\begin{aligned}\mathbf{p}_A(t) &:= c_A \mathbf{v}_A e^{-|A|t} \\ &= |c_A| e^{-|A|t} \begin{pmatrix} 1 \\ -1 \\ -1 \\ 1 \end{pmatrix},\end{aligned} \tag{20}$$

as can be seen from the definition of the eigenvalue A in Eq. (3a) and the expression for c_A in Eq. (16b), the mode is determined only by k_{in} and k_{out} and does not involve k_{tra}. Moreover, the components satisfy

first component: monotonically decreasing = −(second component: monotonically increasing),
third component: monotonically increasing = −(fourth component: monotonically decreasing),

or, equivalently,

$$\begin{aligned}0 > \mathrm{D}\mathbf{p}_{A,1}(t) &= -|Ac_A| e^{-|A|t} = -\mathrm{D}\mathbf{p}_{A,2}(t), \\ 0 < \mathrm{D}\mathbf{p}_{A,3}(t) &= |Ac_A| e^{-|A|t} = -\mathrm{D}\mathbf{p}_{A,4}(t).\end{aligned}$$

Thus, equal amounts of probability are exchanged between states 1 and 2 and between states 3 and 4, respectively. In other words, probability flows from state 1 to state 2, causing the probability of state 1 to decrease by exactly the amount by which that of state 2 increases; the same applies to the exchange between states 3 and 4. Therefore, mode A represents symmetric probability flows that are confined separately to the state-1–state-2 pair and the state-3–state-4 pair. In particular, there is no flow connecting these two pairs of states.

For mode B, namely,

$$\begin{aligned}\mathbf{p}_B(t) &:= c_B \mathbf{v}_B e^{-|B|t} \\ &= |c_B| e^{-|B|t} \begin{pmatrix} 1 \\ -|\alpha| \\ |\alpha| \\ -1 \end{pmatrix},\end{aligned} \tag{21}$$

all three parameters k_{in}, k_{out}, and k_{tra} enter its expression, as in mode C, and the magnitudes of its components show similar temporal changes. The difference from mode C lies in the signs of the components. The sign pattern of the velocity $\mathrm{D}\mathbf{p}_B(t)$ is always $(-,+,-,+)$, which corresponds to probability flows $1 \to 2$, $3 \to 2$, and $3 \to 4$, as indicated by the arrows. Thus, mode B represents flows from state 1 to state 2 and from state 3 to state 4, together with a flow from state 3 to state 2. In the latter flow, the increase in the probability of state 2 is equal to the decrease in the probability of state 3.

Finally, mode 0, namely,

$$\mathbf{p}_0(t) = |c_0|\mathbf{v}_0,$$

is invariant at any time,

$$\mathrm{D}\mathbf{p}_0(t) = 0,$$

and represents the stationary state

$$\mathbf{p}_\infty := c_0\mathbf{v}_0 = \begin{pmatrix} q_\infty \\ r_\infty \\ r_\infty \\ q_\infty \end{pmatrix}, \tag{22}$$

where

$$q_\infty := \frac{1}{2(k_{in}/k_{out}+1)}, \tag{23a}$$

$$r_\infty := \frac{k_{in}/k_{out}}{2(k_{in}/k_{out}+1)}. \tag{23b}$$

The stationary state, namely, a vector $\mathbf{p} \in \sum^4$ satisfying

$$K\mathbf{p} = 0, \tag{24}$$

is given by Eq. (22) and is unique (since $\dim \mathrm{Ker} K = 1$). Any solution with the initial condition in Eq. (15) converges to this point $\mathbf{p}_\infty \in \sum^4$ as $t \to \infty$.

C. Time Evolution of p_4

The state after the permeation is represented by the fourth component p_4 of the solution (6). Since $\mathbf{p}(t)$ takes the form given in Eq. (17) under the initial conditions (15),

expressing the fourth component for each mode yields

$$p_4(t) = p_{04}(t) + p_{A4}(t) + p_{B4}(t) + p_{C4}(t); \tag{25a}$$

$$p_{04}(t) = c_0 k_{out} = q_\infty, \tag{25b}$$

$$p_{A4}(t) = c_A e^{-|A|t},\ p_{B4}(t) = c_B e^{-|B|t},\ p_{C4}(t) = c_C e^{-|C|t}. \tag{25c}$$

Here, each coefficient is only given by parameters k_{in}, k_{out}, k_{tra} as shown in Eq. (3) and Eq. (16).

1. *Sum of Mode C and the Stationary Value*

Let us examine the time evolution in Eq. (25) by assigning specific values to the parameters. Figure 2 shows several cases: a uniform case $k_{in} = k_{out} = k_{tra} =: \bar{k}$, a case in which only k_{tra} is small, and a case in which only k_{in} is large. Other cases are shown in the Supplementary Material (Figs. S1).

In the uniform cases shown in Figs. 2(a) and (b), the dimensionless time evolution is identical, and the only difference is the overall time scale. Indeed, when all three rate parameters are multiplied by a common factor $\gamma > 0$, the time evolution is rescaled as $t \mapsto \gamma t$. This scaling relation holds for all modes. Thus, in the uniform case, $\bar{k}$ determines only the time scale of the system.

In the nonuniform cases, the individual rate parameters affect the time evolution differently. The effect of a small k_{tra} is illustrated by comparing Figs. 2(a) and (c). In Fig. 2(c), the approach of $p_{C4}(t)$ to the stationary value q_∞ is substantially slower than in Fig. 2(a). This is because the smaller value of k_{tra} leads to a smaller magnitude of the eigenvalue C (see Sec. VII). Time evolution of p_4 is strongly affected by that of mode C.

The effects of modes A and B are also evident in Figs. 2(a) and (b). Their contributions suppress the sharp initial rise of $p_4(t)$ that would result from mode C alone. As a result, the actual $p_4(t)$ increases more gradually from zero, with both its first and second derivatives with respect to t vanishing at $t = 0$.

Overall, mode C describes the transient increase of $p_4(t)$ well, while the stationary value $q_\infty = \lim_{t\to\infty} p_4(t)$ is provided by mode 0. Thus, the sum

$$p_{C4}(t) + q_\infty \tag{26}$$

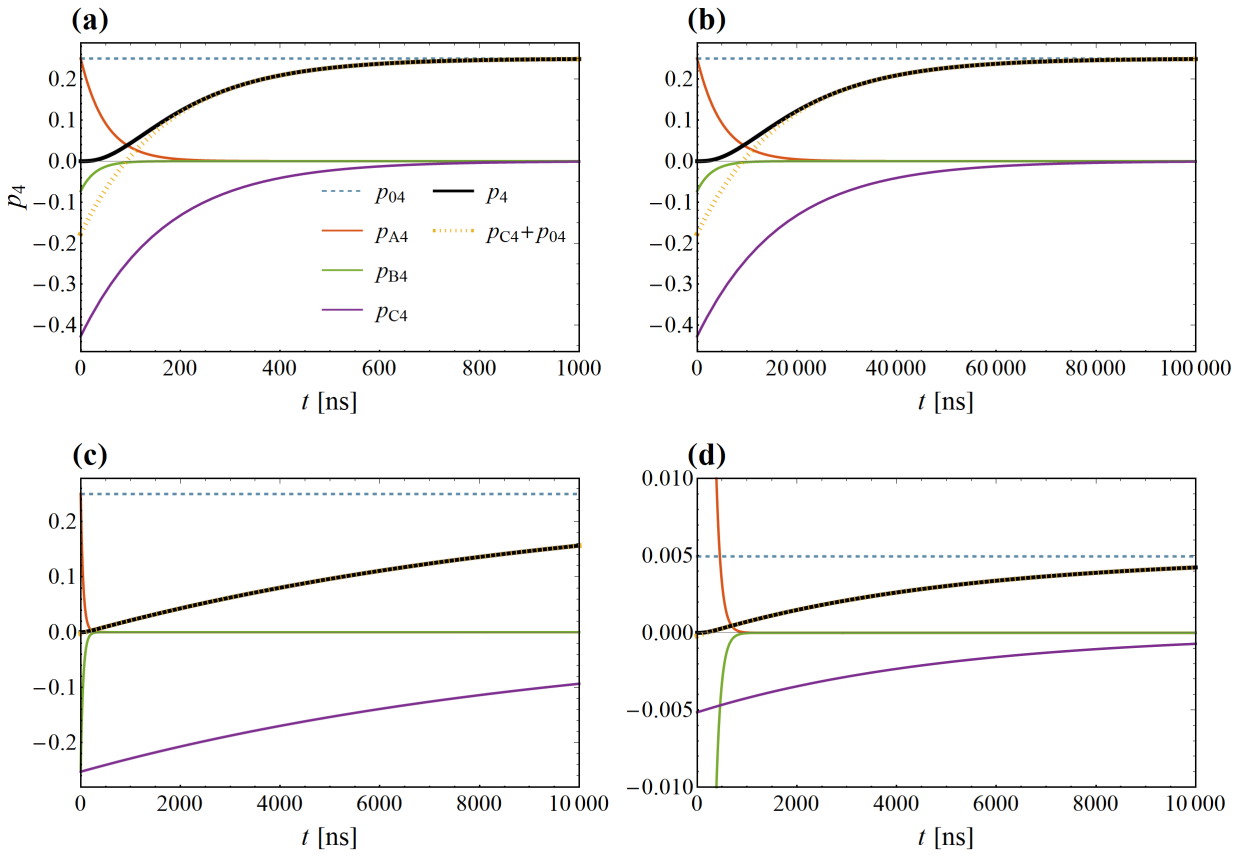


FIG. 2: Time evolutions of the fourth component of the solution, $p_4(t)$, and the fourth components of modes 0, A, B, and C, denoted by $p_{04}(t)$ (mode 0; dashed line), $p_{A4}(t)$ (mode A), $p_{B4}(t)$ (mode B), and $p_{C4}(t)$ (mode C), respectively, as given by Eq. (25), for the initial condition $\mathbf{p}(0) = (1,0,0,0)^T$. The sum $p_{C4}(t)+p_{04}(t)$ (Eq. (26)) is also shown by a dotted line. The rate parameters are (a) $k_{in} = k_{out} = k_{tra} = 0.01\,\mathrm{ns}^{-1}$, (b) $k_{in} = k_{out} = k_{tra} = 0.0001\,\mathrm{ns}^{-1}$, and (c) $k_{in} = k_{out} = 0.01\,\mathrm{ns}^{-1}$ and $k_{tra} = 0.0001\,\mathrm{ns}^{-1}$ and (d) $k_{in} = 0.01\mathrm{ns}^{-1}$ and $k_{out} = k_{tra} = 0.0001\,\mathrm{ns}^{-1}$.

provides a simple approximation to $p_4(t)$. The approximation is less accurate at very early times in case of the uniform rate parameters, where the contributions of modes A and B are important. In contrast, Figs. 2(c) and (d) show that the approximation can remain close to $p_4(t)$ even at early times. A more quantitative analysis of this observation under general initial conditions is given in Sec. VI.

The characteristic time required for $p_4(t)$ to approach the stationary value, as well as that for sum (26), is therefore expected to increase as k_{tra} decreases. In the present cases,

its order of magnitude is approximately given by

$$\tau \approx \frac{1}{k_{tra}}. \tag{27}$$

In molecular dynamics simulations of small molecules, k_{tra} was also found to be on the order of $10^{-7} \sim 10^{-3}\,[\mathrm{ns}^{-1}]$ (Sec. VIII). Thus, τ is estimated to be on the order of $10^3 \sim 10^7\,[\mathrm{ns}]$, corresponding to approximately $1\,[\mu\mathrm{s}] \sim 10\,[\mathrm{ms}]$. This indicates that long-time simulations are generally required to observe membrane permeation.

IV. ANALYSIS OF EXPANSION COEFFICIENTS AND THEIR SIGNS FOR THE INITIAL CONDITION $\mathbf{p}(0) = (a, b, c, 0)^{\mathrm{T}}$

From Sec. III onward, we have assumed as an initial condition that the particle is localized in state 1, i.e., Eq. (15). However, experimentally, there are cases where it is more appropriate to assume that the particles are distributed inside the membrane (states 2 and 3) as the initial condition. We analyze the behavior of the solutions in such cases.

A. Specific Formulas for Expansion Coefficients

By generalizing the initial conditions (15), we have

$$\mathbf{p}(0) = (a, b, c, 0)^{\mathrm{T}}, \tag{28}$$

where

$$a + b + c = 1,\ a, b, c \geq 0. \tag{29}$$

We present the specific expressions for the expansion coefficients of the solution and the results of the sign analysis.

Since the general form of the solution is as shown in Eq. (9), we need only determine the expansion coefficients with respect to the initial conditions (28). This can be done by

substituting Eq. (28) into Eq. (13), yielding

$$\begin{pmatrix} c_0 \\ c_A \\ c_B \\ c_C \end{pmatrix} = \begin{pmatrix} \dfrac{a+b+c}{2(k_{in}+k_{out})} \\ \dfrac{ak_{in}-(b+c)k_{out}}{2(k_{in}+k_{out})} \\ \dfrac{-ak_{in}+2bk_{out}-2ck_{out}+ak_{out}+2ak_{tra}-a\sqrt{D}}{4\sqrt{D}} \\ \dfrac{ak_{in}-2bk_{out}+2ck_{out}-ak_{out}-2ak_{tra}-a\sqrt{D}}{4\sqrt{D}} \end{pmatrix}.$$

These quantities can be more simply represented, by defining

$$G = 2(b-c)k_{out} - a(k_{in} - k_{out} - 2k_{tra}) \tag{30}$$

and noting Eq. (29), such that

$$c_0 = \frac{1}{2(k_{in}+k_{out})} > 0, \tag{31a}$$

$$c_A = \frac{ak_{in}-(1-a)k_{out}}{2(k_{in}+k_{out})}, \tag{31b}$$

$$c_B = \frac{G-a\sqrt{D}}{4\sqrt{D}}, \tag{31c}$$

$$c_C = \frac{-G-a\sqrt{D}}{4\sqrt{D}}. \tag{31d}$$

When compared with the coefficients (16) obtained under the initial conditions (15), only c_0—which concerns the steady state—is the same, while c_A, c_B, and c_C are different.

B. Signs of the Expansion Coefficients

As shown below, the expansion coefficients c_A, c_B, and c_C can have either sign. That is, their signs depend on the values of the parameters k_{in}, k_{out}, and k_{tra} and on the initial conditions a, b, and c. For the special initial condition given by Eq. (15), the signs are fixed as $c_A > 0$, $c_B < 0$, and $c_C < 0$. To demonstrate that the signs are not fixed in general, it would suffice to give examples for which $c_A \leq 0$, $c_B \geq 0$, or $c_C \geq 0$. Here, we present more detailed results.

TABLE I: Possible sign patterns of the expansion coefficients c_A, c_B, and c_C.

Case	c_A	c_B	c_C	Occurrence
(i)	≥ 0	≥ 0	≥ 0	Does not occur
(ii)	< 0	≥ 0	≥ 0	Measure zero
(ii-1)	< 0	> 0	≥ 0	Does not occur
(ii-2)	< 0	$= 0$	> 0	Does not occur
(ii-3)	< 0	$= 0$	$= 0$	Measure zero
(iii)	≥ 0	< 0	≥ 0	Occurs
(iv)	< 0	< 0	≥ 0	Occurs
(v)	≥ 0	≥ 0	< 0	Occurs
(vi)	< 0	≥ 0	< 0	Occurs
(vii)	≥ 0	< 0	< 0	Occurs
(viii)	< 0	< 0	< 0	Occurs

1. *Sign Patterns of c_A, c_B, and c_C*

Classifying each coefficient according to whether it is nonnegative or negative, there are formally eight possible sign patterns. In fact, only the seven patterns except case (i), as indicated in Table I, can occur. In particular, case (ii), as detailed in the classification including cases in which one or more coefficients are zero, occurs only for a set of initial conditions of measure zero. Thus, cases (iii)–(viii) are the six sign patterns that can occur for a set of initial conditions of nonzero measure. A proof is given in Appendix B.

The absence of case (i) means that at least one mode must always have a negative coefficient, which corresponds to a mode contributing to the initial rise of the probability of p_4. This property is physically reasonable. Case (ii) occurs only for a set of initial conditions of measure zero and can therefore be neglected for physical applications.

Thus, the six sign patterns (iii)–(viii) are the practically relevant cases. Since only case (vii) occurs for the typical initial condition (15) corresponding to $(a, c) = (1, 0)$, case (vii) is used as the reference case in the discussions below.

C. Dependence of c_A, c_B, and c_C on the Initial Conditions and Rate Parameters

The set of initial conditions is essentially two-dimensional. Specifically, let Ω_3 denote the set of (a, b, c) satisfying Eq. (29). This set is in one-to-one and onto correspondence with

$$\Omega := \{(a, c) \in \mathbb{R}^2 | \, a, c \geq 0, \ a + c \leq 1\} \tag{32}$$

and thus the set of initial conditions is essentially represented by the triangular region bounded by the coordinate axes and the line $a + c = 1$, including its boundary and interior (see Fig. 3).

Therefore, the dependence of the sign-indefinite coefficients c_A, c_B, and c_C on the initial conditions (a, b, c) is completely characterized by their dependence on the two parameters (a, c). Moreover, their dependence on the rate parameters $k = (k_{in}, k_{out}, k_{tra})$ can also be reduced to two independent parameters. This follows from the fact that c_A, c_B, and c_C are expressed as ratios whose numerators and denominators are both homogeneous of degree one in k. Consequently, these coefficients are invariant under a common scaling of k_{in}, k_{out}, and k_{tra} and depend effectively on only two independent combinations of the three rate parameters. Specifically, scaling with k_{tra} such that

$$r_{in} = k_{in}/k_{tra}, \ r_{out} = k_{out}/k_{tra} \tag{33}$$

enables us to represent the expansion coefficients via the two-dimensional parameter

$$r \equiv (r_{in}, r_{out}) \in \mathbb{R}^2_+ \tag{34}$$

such that

$$\hat{c}_A \equiv \hat{c}_A(a, c; r) = \frac{a r_{in} - (1 - a) r_{out}}{2(r_{in} + r_{out})}, \tag{35a}$$

$$\hat{c}_B \equiv \hat{c}_B(a, c; r) = \frac{\hat{G} - a\sqrt{\hat{D}}}{4\sqrt{\hat{D}}}, \tag{35b}$$

$$\hat{c}_C \equiv c_C(a, c; r) = \frac{-\hat{G} - a\sqrt{\hat{D}}}{4\sqrt{\hat{D}}}, \tag{35c}$$

where

$$\hat{D} \equiv \hat{D}(r) := (r_{in} + r_{out} + 2)^2 - 8 r_{in}, \tag{36a}$$

$$\hat{G} \equiv \hat{G}(a, c; r) := 2(1 - a - 2c) r_{out} - a(r_{in} - r_{out} - 2). \tag{36b}$$

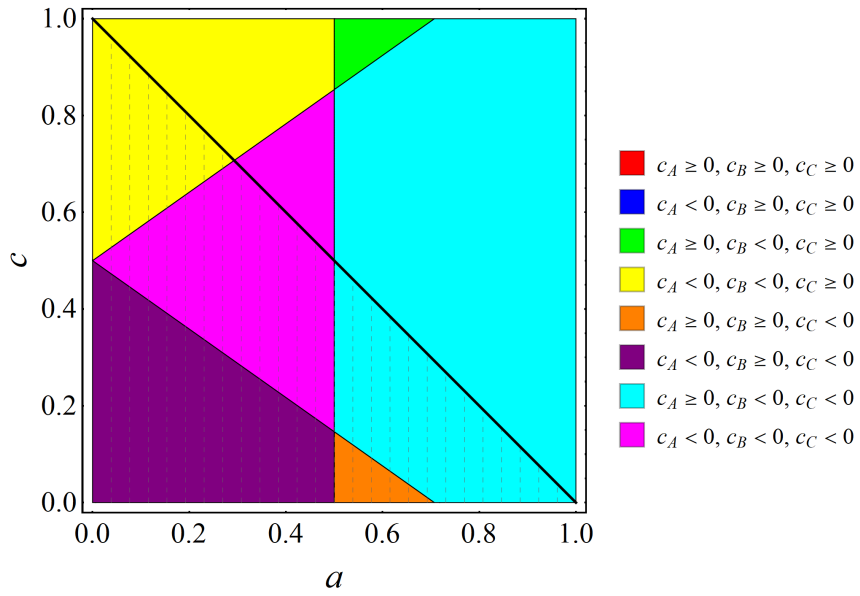


FIG. 3: Sign patterns of c_A, c_B, c_C ($k_{in} = k_{tra} = k_{out}$): The regions in the (a, c) plane corresponding to sign patterns (i)–(viii) are shown in different colors. The uniform case $k_{in} = k_{tra} = k_{out}$ is shown here. The boundaries between the regions are given by three straight lines. The vertical line represents the set of points (a, c) satisfying $c_A = 0$, the upward-sloping line ($c = h'(r)a + \frac{1}{2}$; cf. Eq. (89)) represents the set satisfying $c_C = 0$, and the downward-sloping line (cf. Eq. (90)) represents the set satisfying $c_B = 0$. The dashed lines indicate the triangular domain Ω of the initial conditions. The positions and slopes of these boundary lines, as well as the regions corresponding to the individual sign patterns, depend on the values of the k parameters. Examples for different k-parameter values are shown in the Supplementary Material (Figs. S2). Among the eight possible sign patterns, case (i) does not occur for any values of the k parameters. Case (ii) occurs at the single point $(a, c) = (0, 1/2)$ (see Eq. (81)), corresponding to $c_A < 0$, $c_B = 0$, and $c_C = 0$, whereas this point is not shown in blue. In the uniform case, pattern (iii) (green region) does not occur within Ω.

Here the following relations hold

$$\hat{c}_A(a, c; r) = c_A(a, c; k),\ \hat{c}_B(a, c; r) = c_B(a, c; k),\ \hat{c}_C(a, c; r) = c_C(a, c; k), \tag{37}$$

for which we eliminate b for D, G in Eq. (31) and denote as $c_A \equiv c_A(a, c; k)$, $c_B \equiv c_B(a, c; k)$, and $c_C \equiv c_C(a, c; k)$. Equation (37) indicates that these coefficients are independent of whether they are expressed in terms of the scaled variable r or the original variable k;

this relationship is an intrinsic property of these quantities. The eigenvalues A, B, C and quantities $\sqrt{D}$ and G, in place of such a property, have the following characteristic such as

$$\hat{A} = k_{tra}^{-1} A. \tag{38}$$

D. Time Evolution of p_4 and Each Mode

The fourth component of the solution, p_4, represents the state after permeation. It equals to the fourth component of Eq. (9) even for the initial condition given by Eq. (28). Writing this component in terms of the individual modes gives

$$p_4(t) = p_{04}(t) + p_{A4}(t) + p_{B4}(t) + p_{C4}(t); \tag{39a}$$

$$p_{04}(t) = c_0 k_{out} = q_\infty, \tag{39b}$$

$$p_{A4}(t) = c_A e^{-|A|t},\ p_{B4}(t) = c_B e^{-|B|t},\ p_{C4}(t) = c_C e^{-|C|t} \tag{39c}$$

This expression has the same formal form as Eq. (25). However, here c_A, c_B, and c_C are defined by Eq. (31), whereas A, B, and C retain their definitions in Eq. (3). Thus, except for $p_{04}(t)$, the expressions here differ from those in Eq. (25), as discussed below.

Because the sign patterns of c_A, c_B, and c_C that did not occur for the initial value (15) are now possible, the time evolution of each mode also differs depending on the sign pattern. In particular, a qualitatively different case from those considered above occurs when the sign of mode C is reversed, as in cases (iii) and (iv). Figs. S3 (a) and (b) (Supplementary Material) show the time evolution of each mode for these cases. In these cases, mode C does not primarily represent permeation itself; rather, it reduces an excess increase in $p_4(t)$. In other words, it describes a slow reverse flow from state 4 toward state 3.

In case (vi), the signs of c_A and c_B are interchanged relative to case (vii) (see Fig. S3(d)). In case (viii), all modes have positive coefficients and therefore contribute to an increase in $p_4(t)$ (see Fig. S3(e)).

For case (v) (see Fig. S3(c)), $c_A \geq 0$ and $c_C < 0$ hold, which are the same for case (vii). Therefore, the above discussion of modes A and C in Sec. III B remains valid, because it was based on the signs of the coefficients rather than on their specific values for the initial condition given by Eq. (15). For mode B, on the other hand, its interpretation requires some reconsideration. Nevertheless, the qualitative properties described in Sec. III B remain

valid. In particular, when $c_B > 0$, the sign pattern of $\mathrm{D}\mathbf{p}_B(t)$ is reversed from $(-,+,-,+)$ to $(+,-,+,-)$. Thus, the directions of the probability flows represented by the arrows are reversed, while the qualitative flow pattern of mode B remains unchanged.

Mode 0 is common to all initial values belonging to $\sum^4$, so that it is exactly the stationary state $\mathbf{p}_\infty$ defined in Sec. III B 2. The solution for any initial value $\in \sum^4$ converges to $\mathbf{p}_\infty$ as $t \to \infty$. These follow because the first row of V^{-1} is identical to Eq. (16a) for all four components.

V. RESTRICTIONS ON THE INITIAL CONDITIONS

Thus far, we have considered general initial conditions given by Eq. (28) from a mathematical perspective. However, these conditions include some cases that are not practically expected from a physicochemical perspective. For example, consider the initial condition $(a, b, c) = (0.2, 0.3, 0.5)$. First, in this condition, the total population of target molecules already present inside the membrane is larger than that of molecules outside the membrane before permeation. In preparing a permeation experiment, it is generally not expected that the experiment would be initiated under such a condition. Second, in this condition, the populations in the first and second lipid phases within the membrane are different, as indicated by $(0.3, 0.5)$. Although such a state is physically possible in principle, it would be difficult to detect such a difference experimentally. We acknowledge this potential possibility, but do not consider it further in detail below.

A. Excluded Cases

Regarding the first point, we explicitly exclude initial conditions that substantially deviate from the typical case (vii). This restriction simplifies the subsequent analysis. To implement this restriction systematically among the six sign patterns that can occur, we define the excluded cases as follows:

- A case is excluded if its region in the sign-pattern diagram (Fig. 3) shares only a point with the region corresponding to case (vii).

As shown in Fig. 3 and proved in Appendix C, the above definition is determined by a topological property of the (a, c) space and does not depend on the values of the k parameters.

When $h'(r)$ (the slope of the upward-sloping line) in Eq. (89) or $|g'(r)|$ (the absolute value of the slope of the downward-sloping line) in Eq. (90) is large, and the right-hand side of Eq. (83) (the a-coordinate of the vertical line) is also large, the topology may change; but in such cases, case (iii) or case (v) simply disappears automatically, which is fully consistent with the exclusion scheme described above.

According to this definition, the two cases that should be excluded are

- case (iv): a is small and c is large;
- case (vi): a is small and c is also small, and hence b is large.

Thus, we adopt the following policy:

Policy 1 We impose conditions on the parameters so that cases (iv) and (vi) are excluded.

A common feature of cases (iv) and (vi) is that a is small. This is consistent with the above rationale for excluding cases that are far from case (vii). Accordingly, based on the same rationale, we also consider the possibility of excluding other parameter regions. Specific conditions are introduced in the following subsection.

B. Realization of Policy 1

To realize Policy 1, we assume the following condition

Condition 1 (Assumption)

$$a \geq \frac{1}{\min\{1, r_{in}/r_{out}\} + 1} =: a_{\min}. \tag{40}$$

This assumption can be rephrased as follows:

$$a \geq a_{\min} \Leftrightarrow \left\{ \begin{array}{ll} a \geq \frac{1}{2} & \text{-(a)} \\ \text{and} & \\ a \geq \dfrac{1}{r_{in}/r_{out} + 1} & \text{-(b)} \end{array} \right\}. \tag{41}$$

Now, under Condition 1, it follows that (proved in Appendix C)

Proposition 2 *Eq. (40)* $\Rightarrow c_A \geq 0$, $c_C < 0$.

The sign pattern $c_A \geq 0$ and $c_C < 0$ is satisfied only by cases (v) and (vii). Therefore, under Assumption (1), cases (iii), (iv), (vi), and (viii) are excluded. As noted above, cases (i) and (ii) are ignored because they occur only for sets of initial conditions of measure zero. Thus, Policy 1 is realized.

In addition to the two cases that were intended to be excluded, namely, cases (iv) and (vi), cases (iii) and (viii) are also excluded. However, this does not constitute an unnecessarily restrictive exclusion. First, the occurrence of case (iii) requires $c_C \geq 0$. As shown by Eq. (89) in the proof of Proposition 2, this condition implies $c > 1/2$ and hence $a < 1/2$. In this respect, case (iii) is similar to case (iv), which is to be excluded.

Next, the occurrence of case (viii) requires $c_A < 0$. As shown by Eq. (83) in the proof of Proposition 2, this case can occur only when $a < \dfrac{1}{r_{in}/r_{out} + 1}$. For the systems of practical interest, as shown in Sec. VIII C, $r_{in} > r_{out}$ holds for many molecules. Consequently, case (viii) corresponds in most cases to a situation with only a very small value of a. Therefore, as discussed in Sec. V A, excluding this case is also considered reasonable.

In summary, the cases considered in the following analysis, which we denote by "Case (O)," are limited to cases (v) and (vii). They can be characterized solely by the signs of c_A and c_C:

$$\text{Case (O)} : \text{case (v) or case (vii)} \Longleftrightarrow c_A \geq 0 \text{ and } c_C < 0. \tag{42}$$

Thus, by setting the parameters so as to satisfy Condition 1, Policy 1 is realized.

Note that *under condition* $a \geq \frac{1}{2}$, which is a condition without using parameter r and also a necessary condition for Condition 1, the following equivalence holds:

$$\begin{aligned} \text{Case (O)} &\Leftrightarrow a \geq a_{\min} \Leftrightarrow a \geq \frac{1}{r_{in}/r_{out} + 1} \left(= \frac{1}{k_{in}/k_{out} + 1} = 2q_\infty \right) \\ &\Leftrightarrow r_{in} \geq (1/a - 1) r_{out}. \end{aligned} \tag{43}$$

For practical use, a simpler condition may be more convenient. The following condition is a sufficient condition for Condition 1:

Condition 3 (Strong assumption)

$$a \geq \frac{1}{2}, \quad k_{in} \geq k_{out}. \tag{44}$$

Remark 4 *The Strong Assumption corresponds to an experimental setting in which target molecules satisfying $k_{in} \geq k_{out}$ are used and the initial fraction of the molecules in state 1, a, is set to at least one half of the total molecular population. In other words, the initial concentration of molecules that have already entered the membrane need not be zero, but it should be less than one half of the total concentration. The condition $k_{in} \geq k_{out}$ does not necessarily need to be known for each individual molecule in advance. If this inequality is empirically satisfied for a given group of molecules, the condition can be adopted without determining k_{in} and k_{out} separately before performing the calculation or experiment.*

Remark 5 *The original assumption [Condition 1] is less restrictive and also allows the use of target molecules for which $k_{in} < k_{out}$. In this case, however, a more restrictive initial condition is required. Specifically, a must satisfy*

$$a \geq \frac{1}{k_{in}/k_{out} + 1} \left(> \frac{1}{2} \right),$$

so that the initial fraction of the molecules in state 1 is sufficiently large, or equivalently, the initial population outside the membrane is sufficiently dominant. For example, when $k_{out} = 10k_{in}$, this condition requires $a \geq 0.909$. Thus, the original assumption allows greater freedom in the choice of molecules at the expense of imposing a more restrictive initial condition. For the molecules examined in this study, $k_{in} \geq k_{out}$ was satisfied (see Sec. VIII).

VI. RESTRICTION OF THE PARAMETER REGION

We now ask whether the long-lived mode C can be regarded as the mode that represents the permeation behavior, for which p_4 is well approximated, in the cases belonging to Case (O). Although this may appear intuitive, a counterexample has in fact been found. An example is shown in Fig. S1(d) for $k_{in} = k_{tra} = 0.01$, and $k_{out} = 0.0001$. In this case, none of the individual modes provides a particularly good approximation to $p_4(t)$. Mode C has too large absolute amplitude at the initial time, so that it does not well approximate p_4. When the stationary mode 0 is added as an offset, mode B nevertheless provides a closer approximation to $p_4(t)$ than mode C.

A. Strategies

Therefore, we seek to identify appropriate conditions on the rate parameters k and the initial values such that mode C becomes the principal mode governing permeation. The reason for treating mode C as special is that it is the longest-lived mode, and, as discussed in Sec. III B, it is the mode most naturally associated with permeation under the ideal initial condition given by Eq. (15).

As discussed in Sec. IV C, the independent parameters that characterize the signs of c_A, c_B, and c_C can be taken to be the initial variables (a, c) and the rate parameters $r \equiv (r_{in}, r_{out})$ normalized by k_{tra}. Thus, our objective is defined as follows.

Objective: To identify appropriate conditions on the range of the four parameters (a, c, r_{in}, r_{out}) such that mode C determines the permeation behavior.

Before specifying the appropriate conditions, they should satisfy at least the following requirements:

- they should cover a sufficiently broad range of conditions;
- they should be practically usable, in the sense that their validity should not be difficult or cumbersome to determine.

These requirements are important for the initial conditions, because they correspond to the conditions under which a system is prepared before an experiment is initiated. That is, conditions that are too restrictive or difficult to realize are therefore not practical. Ideally, the initial conditions should also be capable of representing situations that mimic those in actual biological systems. The two requirements are desirable for the rate parameters k, because they may provide useful guidelines for molecular design.

We therefore investigate which of modes A, B, and C, when combined with mode 0, satisfies the following criterion:

Problem 6 ***Which mode provides the best approximation to the exact solution while representing the permeation process?***

Here, mode 0 is the common stationary value for arbitrary initial conditions. Adding mode 0 is necessary because it brings the long-time behavior of each individual mode toward the stationary value of p_4 as $t \to \infty$.

From this perspective, the relative suitability of the three modes is determined by the following factors:

(a) **The mode is an increasing mode:**

A decreasing mode does not represent permeation. Thus, the expansion coefficient involved in the mode should be negative.

(b) **The mode describes the long-time behavior well:**

In this respect, mode C, which has the smallest $|C|$, is clearly advantageous because it is the longest-lived mode.

(c) **The mode describes the initial increase of the exact solution well:**

Not only the long-time behavior but also the initial behavior should be closest, among the modes, to p_4. In this respect, the mode with the largest absolute intercept, which is not necessarily mode C, may provide the best description of the initial behavior. Indeed, as shown, for example, in Fig. 2(d), when $k_{in} > k_{tra}, k_{out}$, the absolute amplitudes of modes A and B at the initial time are larger than that of mode C. However, because this consideration must be balanced against condition (b), the mode with the largest absolute intercept alone cannot determine the answer to Problem 6; further analysis is required. The absolute intercepts of modes A, B, and C are given by $|c_A|$, $|c_B|$, and $|c_C|$, respectively, since these are their amplitudes at the initial time.

In Case (O), mode C already satisfies conditions (a) and (b). Therefore, to achieve the objective of restricting the parameter region, we adopt the following policy:

Policy 2 Within Case (O), we further restrict the parameter region so that mode C also satisfies condition (c).

In other words, we first impose Condition 1 to realize Case (O). We then focus on mode C, which already satisfies conditions (a) and (b), and investigate how the parameter region can be further restricted so that mode C also satisfies condition (c). This procedure leads to a further narrowing of the parameter region.

B. Realization of Policy 2

In Case (O), mode A represents a decreasing contribution and therefore does not satisfy condition (a). Thus, the modes to be considered are modes B and C. To realize Policy 2, we take the following approach:

(I) Define an evaluation function R_∞ that quantifies the extent to which mode C satisfies condition (c) relative to mode B based on the function value;

(II) Use R_∞ to identify a parameter region, in a simple and convenient form, in which mode C can be regarded as satisfying condition (c).

1. Realization of Approach (I)

For (I), the evaluation function is defined as the ratio of the integral over all time of the deviation from the exact solution p_4. Specifically, for mode C, the deviation of p_{C4} from p_4—after adding the offset p_{04} to p_{C4}—can be calculated with a help of the fact that $p_4 - (p_{C4} + p_{04}) = p_{A4} + p_{B4}$, which comes from Eq. (39a), such that

$$\delta_\infty^C := \|p_4 - (p_{C4} + p_{04})\|_1 = \|p_{A4} + p_{B4}\|_1 := \int_0^\infty \left| c_A e^{At} + c_B e^{Bt} \right| \, dt. \tag{45}$$

This serves as the indicator for mode C. Similarly, the the indicator for mode B becomes

$$\delta_\infty^B := \|p_4 - (p_{B4} + p_{04})\|_1 = \int_0^\infty \left| c_A e^{At} + c_C e^{Ct} \right| \, dt. \tag{46}$$

We define the following ratio as the evaluation function:

$$R_\infty \equiv \frac{\delta_\infty^C}{\delta_\infty^B} \tag{47}$$

Criterion 7 *We regard mode C as satisfying condition (c) when*

$$R_\infty < 1. \tag{48}$$

By definition, R_∞ is nonnegative. Moreover, all quantities appearing in R_∞ can be expressed solely in terms of (a, c, r): c_A, c_B, and c_C are given by Eq. (37), while the dependence on A, B, and C can be expressed in terms of r using Eq. (38), where the factor k_{tra} cancels from the use of a scaled time $t' = k_{tra}t$ and from Eq. (47). For simplicity, we write R_∞ without explicitly indicating its dependence on (a, c, r).

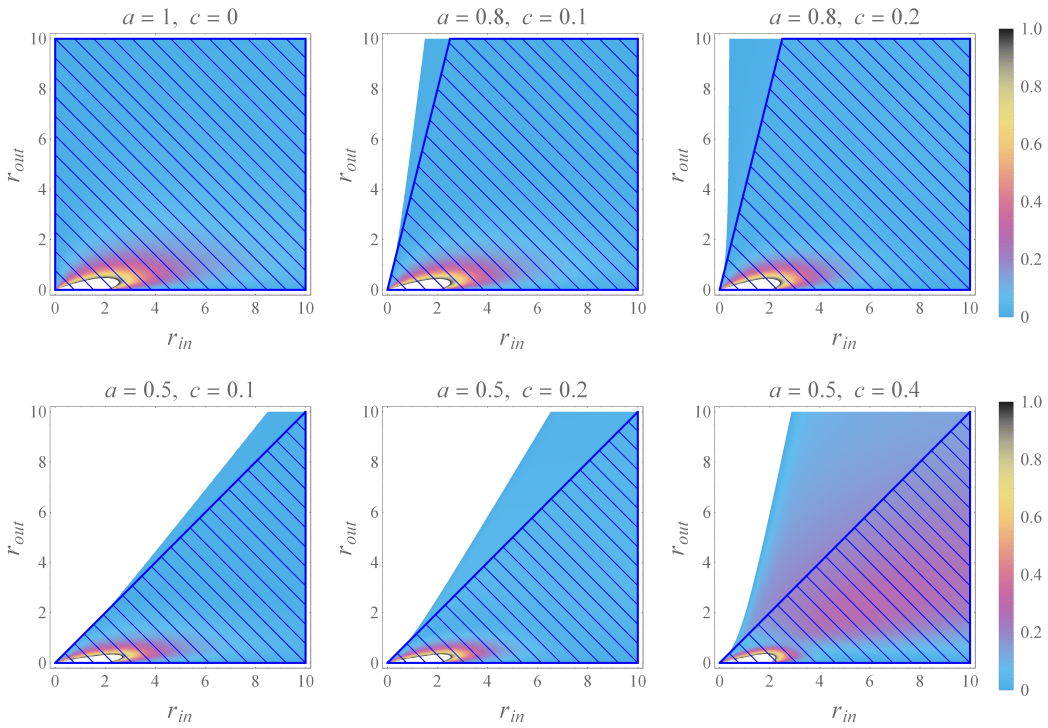


FIG. 4: For each value of (a, c), the value of $R_\infty = R_\infty(a, c, r)$ is shown in the (r_{in}, r_{out})-plane. The color intensity represents the value of R_∞, restricted to the range $[0, 1]$, as indicated by the color scale on the right. The blue-hatched region indicates the region satisfying $r_{in} \geq (1/a - 1)r_{out}$.

2. *Realization of Approach (II)*

Approach (II) can be realized by investigating the range of the parameters a, c, and r for which $R_\infty < 1$. For this purpose, we performed numerical calculations.

Under condition $a \geq \frac{1}{2}$, which is a necessary condition for Condition 1, we considered $a = 1$, 0.8, and 0.5, and varied c over the range $0 \leq c \leq 1 - a$. The results are plotted in Fig. 4. Results over a wider parameter range (Fig. S4) and for other values of a (Fig. S5) are shown in the Supplementary Material. For each (a, c), the region in the two-dimensional (r_{in}, r_{out}) space in which $R_\infty = R_\infty(a, c, r)$ takes values less than or equal to 1 is represented by a color gradient.

The blue hatched region indicates Case (O), namely, the region satisfying $r_{in} \geq (1/a - 1)r_{out}$ (see Eq. (43))). This region becomes wider as a increases. For $(a, c) = (1, 0)$, which is the largest possible value of a, only case (vii), which is a subset of Case (O), occurs, and therefore the entire plotted region is hatched. For c, there is a tendency for R_∞ to increase

as c increases.

The region relevant to the realization of Policy 2 is the part of Case (O), namely, the hatched region in the figure, in which mode C satisfies condition (c), that is, $R_\infty < 1$. The region with $R_\infty \geq 1$ is therefore an exceptional region in which mode C does not satisfy condition (c), and is shown as an uncolored region in the figure.

This exceptional region can be divided into two distinct regions. The first is a vertically elongated region at small r_{in} that extends over a wide range of r_{out}. This region tends to become wider as a or c decreases. However, this first exceptional region lies outside Case (O) and therefore does not affect the realization of Policy 2.

The second exceptional region, which is relevant here, is an uncolored region with the characteristic shape in the lower-left part of the parameter space, approximately $0 \lesssim r_{in} \lesssim 2.5$ and $0 \lesssim r_{out} \lesssim 0.5$. This region tends to extend further in the r_{in} direction as c decreases and further in the r_{out} direction as a increases. Because this second exceptional region is contained within Case (O), it must be excluded according to Approach (II). For points (r_{in}, r_{out}) in this second exceptional region, mode B provides a closer approximation to the exact solution than mode C. For example, as shown in Fig. S1(d), mode B has a smaller initial deviation from the exact solution than mode C.

These numerical results suggest that the following condition can be adopted for the realization of Approach (II):

$$r_{out} \gtrsim 1/2 \quad \text{or} \quad r_{in} \gtrsim 3 \tag{49}$$

In addition, to avoid the small exceptional behavior associated with the boundary of the applicable region, we impose a small margin on Eq. (40), namely, $a \geq a_{\min} + \delta$ for a certain small $\delta > 0$. In practical terms, we use the simpler condition

$$a \gtrsim a_{\min}. \tag{50}$$

These conditions are sufficiently simple for practical use.

Summary–. Under the conditions given by Eqs. (49) and (50), mode C is an increasing mode and provides a good description of both the initial and long-time behavior of the exact solution p_4. Therefore, under these conditions, $|C|$, which is the inverse of the relaxation time and has the physical dimension of a rate, can be used to characterize the permeation rate.

VII. PARAMETER DEPENDENCE AND ASYMPTOTIC BEHAVIOR

The preceding analysis has shown that, under the conditions given by Eqs. (49) and (50), the permeation rate s can be considered proportional to $|C|$:

$$s \propto |C|. \tag{51}$$

Below, we refer to $|C|$ as the permeation rate, with the proportionality constant omitted. In this section, we analyze C as a function of the three rate parameters $k \equiv (k_{in}, k_{tra}, k_{out})$.

A. Parameter Dependence

This subsection focuses on the asymptotic behavior and monotonicity of C with respect to each parameter. All proofs of equations [Eqs. (52)–(63) and Table II] are given in Appendix D.

1. Dependence on k_{tra}

In the regime $k_{tra} \ll k_{in}, k_{out}$, C is approximated to first order as

$$C \approx -\frac{2k_{in}}{k_{in} + k_{out}} k_{tra}. \tag{52}$$

Thus, in this regime, C is proportional to k_{tra}, and the proportionality coefficient is determined by the relative magnitudes of k_{in} and k_{out}. In fact, the approximation holds over a broader parameter range, as Fig. 5(a). In particular, when k_{in} and k_{out} are of comparable magnitude, $C \approx -k_{tra}$ (see Fig. 5(b)), indicating that k_{tra} is the dominant factor, or bottleneck.

Conversely, consider the regime $k_{tra} \gg k_{in}, k_{out}$. As k_{tra} increases, C approaches

$$C \approx -k_{in}. \tag{53}$$

See Fig. 5(c) for this approximation. In this regime, C becomes independent of the transport rate k_{tra} and the efflux rate k_{out}, and its value is determined by the influx rate k_{in}.

The above results show that $|C|$ is proportional to k_{tra} when k_{tra} is sufficiently small (Eq. (52)) and approaches a constant value as k_{tra} increases (Eq. (53)). This suggests that $|C|$ increases with increasing k_{tra}. Indeed, $|C|$ is a monotonically increasing function of k_{tra}:

$$\frac{\partial |C|}{\partial k_{tra}} > 0 \quad \text{for all } k_{in}, k_{out}, k_{tra} > 0. \tag{54}$$

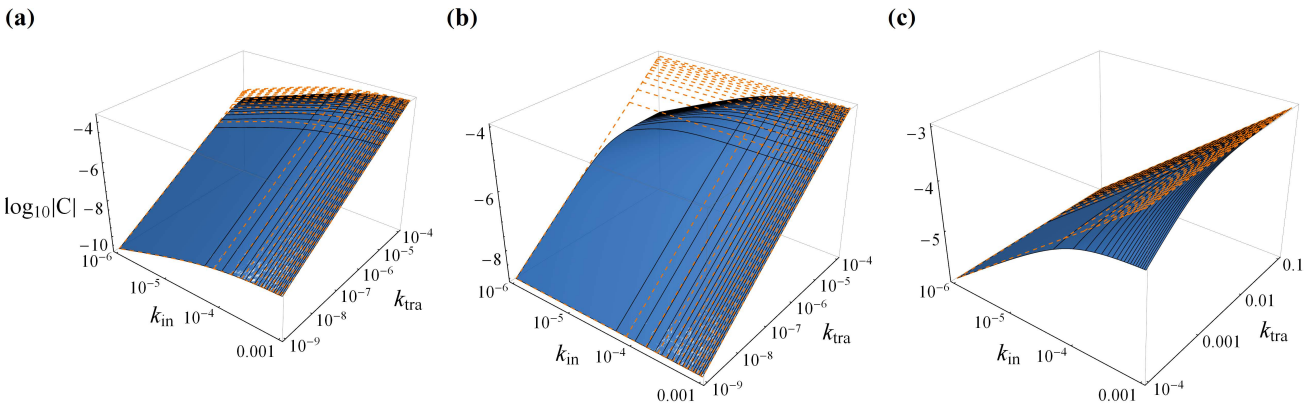


FIG. 5: Asymptotic behavior of the eigenvalue magnitude $|C|$ for different rate-parameter regimes. The exact results depicted by the colored surfaces with the solid lines are compared with the corresponding asymptotic approximations dipicted by the surfaces with dashed lines. (a) $k_{out} = 10^{-4}$ is fixed: approximation (52) holds for $k_{tra} \ll k_{in}, k_{out}$; (b) $k_{in} = k_{out}$ case: approximation $|C| \approx k_{tra}$ (see Eq. (52)) holds for $k_{tra} \ll k_{in}, k_{out}$; (c) $k_{in} = k_{out}$ case: approximation (53) holds for $k_{tra} \gg k_{in}, k_{out}$.

2. *Dependence on k_{in}*

To examine the dependence of C on k_{in}, we first note a symmetry of C. Specifically, C is invariant under the following rescaled interchange of k_{in} and k_{tra}:

$$(k_{in}, k_{tra}) \leftrightarrow \left(2k_{tra}, \tfrac{1}{2}k_{in}\right). \tag{55}$$

Thus, the properties of C with respect to k_{in} can be derived from those with respect to k_{tra}. In contrast, no similarly apparent symmetry of C involving k_{out} is found.

First, consider the regime $k_{in} \ll k_{out}, k_{tra}$. In this regime,

$$C \approx -\frac{2k_{tra}}{k_{out} + 2k_{tra}} k_{in}. \tag{56}$$

Thus, when k_{in} is small, C varies proportionally to k_{in}, corresponding to an influx-limited regime. Defining $\gamma = \frac{k_{out}}{2k_{tra}} > 0$,we obtain

$$|C| \approx \frac{k_{in}}{1+\gamma},$$

so that increasing k_{tra} or k_{out} does not remove the limitation.

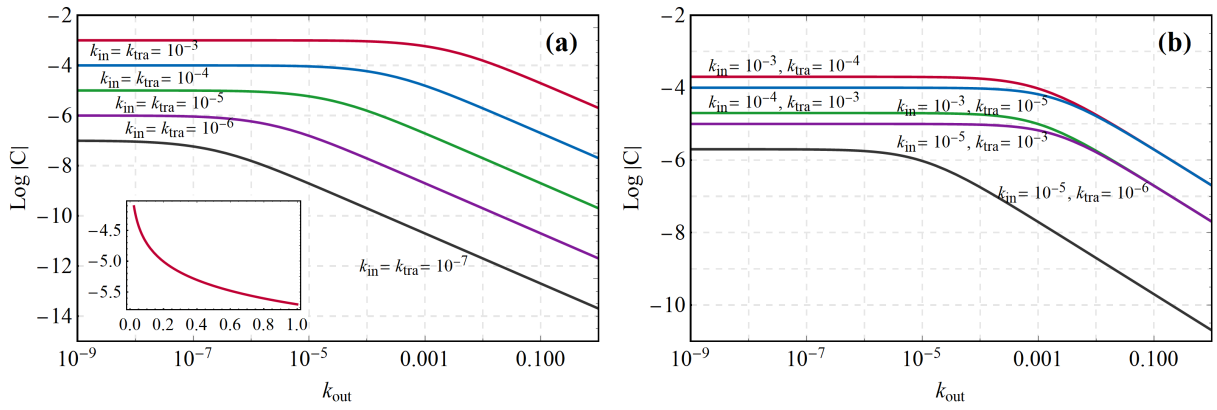


FIG. 6: Dependence of $|C|$ on k_{out}: (a) Results for five different values of $k_{in} = k_{tra}$ are shown. As k_{out} decreases, $|C|$ approaches the constant value k_{in} given by Eq. (59) (log–log scale). The inset shows $|C|$ (red solid line) and the approximate curve given by Eq. (60) (black dotted line) on a linear scale, for $k_{in} = k_{tra} = 10^{-3}$. (b) Results for five different combinations of k_{in} and k_{tra}, with $k_{in} \neq k_{tra}$, is shown.

Conversely, consider the regime $k_{in} \gg k_{out}, k_{tra}$. In this regime,

$$C \approx -2k_{tra}. \tag{57}$$

Thus, when k_{in} is large, C approaches the value $-2k_{tra}$ and becomes independent of k_{in}. In other words, the overall rate is limited by the transport capacity $2k_{tra}$, and the influence of k_{in} vanishes. This transport-limited regime is discussed in more detail in Sec. VII B 3.

As in the case of k_{tra}, $|C|$ is a monotonically increasing function of k_{in}:

$$\frac{\partial |C|}{\partial k_{in}} > 0 \quad \text{for all } k_{in}, k_{out}, k_{tra} > 0. \tag{58}$$

3. *Dependence on k_{out}*

Consider first the regime $k_{out} \ll k_{in}, k_{tra}$. In this regime,

$$C \approx -\min\{k_{in}, 2k_{tra}\}. \tag{59}$$

Thus, C approaches a value that is independent of k_{out} (see Fig. 6(a)). In other words, when k_{out} is very small and efflux is almost absent, the smaller of k_{in} and $2k_{tra}$ effectively determines the bottleneck.

Conversely, when $k_{out} \gg k_{in}, k_{tra}$,

$$C \approx -\frac{2k_{in}k_{tra}}{k_{out}}. \tag{60}$$

Thus, when k_{out} is large, C is inversely proportional to k_{out} and approaches zero (see Fig. 6(a): inset). The decrease in the permeation rate, which is proportional to $|C|$, can be understood primarily in terms of the influx side rather than the efflux process. Specifically, after a target molecule reaches state 2, a large k_{out} increases the rate at which it is returned to state 1 before it has an opportunity to proceed to state 3. Consequently, the probability of reaching state 3 by overcoming the central transport step characterized by k_{tra} is reduced.

The above results show that $|C|$ approaches a constant value when k_{out} is sufficiently small (Eq. (59)) and decreases inversely with k_{out} as k_{out} becomes large (Eq. (60)). This suggests that $|C|$ decreases with increasing k_{out}. Indeed, $|C|$ is a monotonically decreasing function of k_{out}:

$$\frac{\partial |C|}{\partial k_{out}} < 0 \quad \text{for all } k_{in}, k_{out}, k_{tra} > 0. \tag{61}$$

4. Summary of the Parameter Dependence

The asymptotic behavior and limiting values of C when each parameter is much larger or smaller than the other two are summarized in Table II.

TABLE II: Summary of the asymptotic behavior of C and the dominant factors

Parameter	Condition	Approximation for C	Limit of C	Dominant factor
k_{tra}	$k_{tra} \to 0$	$-\frac{2k_{in}}{k_{in}+k_{out}}k_{tra}$	0	k_{tra}
	$k_{tra} \to \infty$	$-k_{in}$	$-k_{in}$	k_{in}
k_{in}	$k_{in} \to 0$	$-\frac{2k_{tra}}{k_{out}+2k_{tra}}k_{in}$	0	k_{in}
	$k_{in} \to \infty$	$-2k_{tra}$	$-2k_{tra}$	k_{tra}
k_{out}	$k_{out} \to 0$	$-\min\{k_{in}, 2k_{tra}\}$	$-\min\{k_{in}, 2k_{tra}\}$	k_{in} or k_{tra}
	$k_{out} \to \infty$	$-\frac{2k_{in}k_{tra}}{k_{out}}$	0	k_{out}

The above analysis leads to the following conclusions regarding the influence of the three rate parameters on $|C|$.

1. **When the transport rate k_{tra} is influential:** This occurs when k_{tra} is small or when k_{in} is very large. In this regime, the overall process is limited by transport within the membrane.

2. **When the influx rate k_{in} is influential:** This occurs when k_{in} is small or when k_{tra} is very large. In this regime, the supply of molecules to the system is limiting.

3. **When the efflux rate k_{out} is influential:** This occurs when k_{out} is very large. In this regime, a large k_{out} enhances the return of molecules from state 2 to state 1, thereby reducing the probability that they proceed to state 3 and lowering the overall permeation rate.

5. Range of $|C|$

A simple expression $\min\{k_{in}, 2k_{tra}\}$ provides an upper bound for $|C|$ for given values of k_{in} and k_{tra}:

$$|C| < \min\{k_{in}, 2k_{tra}\}. \tag{62}$$

This relation is discussed in more detail in Sec. VII B 2. It should be noted that Eq. (62) does not claim that $|C|$ itself is bounded (see also Sec. IX) and only specifies an ordering relation among the three quantities $|C|$, k_{in}, and $2k_{tra}$. The range of possible values of $|C|$ is

$$0 < |C| < \infty, \tag{63}$$

where $|C|$ can be made arbitrarily large by increasing k_{in} and k_{tra} simultaneously.

B. Strategies for Increasing $|C|$

In this subsection, based on discussions so far, we examine how to increase the permeation rate $|C|$ and derive an approximate expression for $|C|$ that helps achieve this efficiently.

1. General framework

a. Dependence on k_{tra} and k_{in} When either k_{tra} or k_{in} is small, C depends strongly on the parameter of the slowest process, which acts as the bottleneck. Increasing the other

parameters does not substantially improve the overall rate $|C|$. Conversely, when only one of k_{tra} and k_{in} is increased, the other parameter determines the overall rate. That is, increasing k_{in} while keeping k_{tra} small, or increasing k_{tra} while keeping k_{in} small, does not lead to a large value of $|C|$ (Table II). Therefore, to increase $|C|$, both k_{tra} and k_{in} should be increased.

b. Dependence on k_{out} The dependence of C on k_{out} is different. Even when k_{out} is small, $|C|$ can be increased if both k_{tra} and k_{in} are large. In other words, although the efflux from state 4 is slow, the return to state 1 is also slow, and therefore $|C|$ can be increased by increasing both k_{tra} and k_{in}. In contrast, as k_{out} increases, the return to state 1 becomes faster, resulting in a decrease in $|C|$.

c. Summary of the Parameter Dependence In summary, $|C|$ can be increased by making both k_{tra} and k_{in} large while keeping k_{out} small. The former is discussed quantitatively in the remainder of this subsection, whereas the latter is reconsidered in Sec. IX.

2. Possibility of Determining $|C|$ Solely from k_{tra} and k_{in}

Eq. (59) is an approximation valid for sufficiently small k_{out}. However, as suggested by Fig. 6(a), there are regions in which $|C|$ is nearly independent of k_{out} and Eq. (59) provides a good approximation even when k_{out} is not particularly small, depending on the values of k_{tra} and k_{in}. In other words, as k_{out} decreases, $|C|$ gradually approaches the value $\min\{k_{in}, 2k_{tra}\}$ appearing in Eq. (59), and a plateau is formed when k_{out} becomes sufficiently small.

Example 8 *For example, when*

$$k_{in} \approx k_{tra} \gtrsim 10^{-4}\,[\mathrm{ns}^{-1}], \tag{64}$$

as shown in Fig. 6(a), decreasing k_{out} from a large value to approximately 10^{-4} contributes to an increase in $|C|$. However, further decreasing k_{out} below 10^{-4} produces little change in $|C|$. In other words, if

$$k_{out} \lesssim 10^{-4} \tag{65}$$

and Eq. (64) are assumed, the dependence of $|C|$ on k_{out} becomes weak, and $|C|$ can be approximated by $\min\{k_{in}, 2k_{tra}\}$.

In such a plateau region, there is no need to design the system specifically to reduce k_{out}. Rather, increasing k_{tra} and k_{in} should be the primary focus when seeking to increase $|C|$.

Example 9 *As another example, consider the case in which k_{in} and k_{tra} are not necessarily comparable. If*

$$\min\{k_{in}, k_{tra}\} \gtrsim 10^{-5}, \tag{66}$$

as shown in Fig. 6(b), and if Eq. (65) is satisfied, the dependence of $|C|$ on k_{out} is weak, and Eq. (59) provides a reasonable approximation.

We now examine this behavior more quantitatively and systematically. Specifically, we investigate when and to what extent $\min\{k_{in}, 2k_{tra}\}$ approaches $|C|$ over the entire parameter space. For a prescribed error tolerance δ, we consider the parameter region satisfying

$$\left| \frac{|C| - \min\{k_{in}, 2k_{tra}\}}{\min\{k_{in}, 2k_{tra}\}} \right| \leq \delta. \tag{67}$$

Within this region, the absolute difference between $|C|$ and its approximation $\min\{k_{in}, 2k_{tra}\}$ is at most δ times the approximation value. Because $\min\{k_{in}, 2k_{tra}\}$ is given simply by either k_{in} or $2k_{tra}$, this approximation may also provide a useful guideline for molecular design.

Moreover, Eq. (67) can be reduced to a dimensionless form by scaling the rate parameters by k_{tra}. Specifically, defining

$$s(r) := \left| \frac{|\hat{C}| - \min\{r_{in}, 2\}}{\min\{r_{in}, 2\}} \right|, \tag{68}$$

Eq. (67) is equivalent to $s(r) \leq \delta$. Thus, the error can be evaluated solely as a function of $r = (r_{in}, r_{out})$, which considerably simplifies the analysis. Indeed, the following relation holds (see Appendix E for the proof):

Proposition 10 *For any $r = (r_{in}, r_{out}) \in \mathbb{R}^2_+$, it holds that $0 < s(r) < 1$ and that for any $\delta \in (0, 1)$,*

$$\textit{(i)} \quad s(r) \leq \delta \iff \left\{ \begin{array}{ll} r_{out} \leq \frac{\delta}{1-\delta} r_{in} - 2\delta & \textit{if } r_{in} > 2 \\ r_{out} \leq -\delta r_{in} + \frac{2\delta}{1-\delta} & \textit{if } r_{in} \leq 2 \end{array} \right\}, \tag{69a}$$

$$\textit{(ii)} \quad r_{in} \geq r_{out} \Rightarrow s(r) \leq s(2,2) = (\sqrt{5} - 1)/2, \tag{69b}$$

$$\textit{(iii)} \quad r_{in} \geq r_{out},\ r_{in} \geq 2\lambda,\ \lambda \geq 1 \ \Rightarrow s(r) \leq \delta_\lambda \equiv s(2\lambda, 2\lambda), \tag{69c}$$

$$\textit{where } \delta_\lambda \textit{ is decreasing with increasing } \lambda \textit{ and } \lim_{\lambda \to \infty} \delta_\lambda = 1/2. \tag{69d}$$

For part (i), the equality $s(r) = \delta$ corresponds to the case in which the equality holds in both of the linear inequalities appearing on the right-hand side of part (i). Thus, the

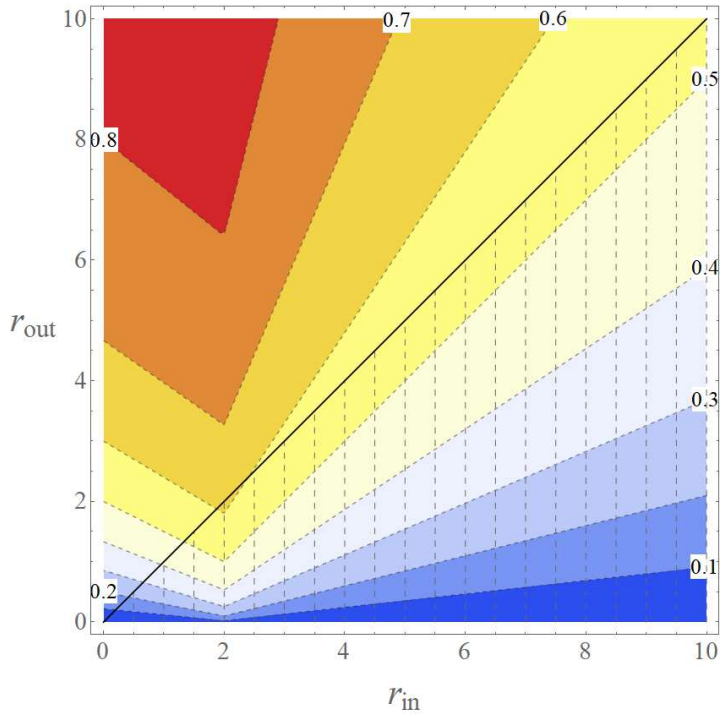


FIG. 7: Contour of the error $s(r_{in}, r_{out}) \in (0, 1)$, where $\min\{r_{in}, 2\}$ approximates the factorized permeation rate $|\hat{C}|$. The dashed lines indicate the region $r_{in} \geq r_{out}$, where $s(r) \leq s(2, 2) \approx 0.618$.

level curves of the error $s(r)$ are given by remarkably simple piecewise-linear expressions. Specifically, for $r_{in} > 2$, the level curve is given by the upper expression in part (i) and is a straight line with positive slope $\delta/(1-\delta)$, whereas for $r_{in} \leq 2$, it is given by the lower expression and is a straight line with negative slope $-\delta$ (Fig. 7). Thus, as suggested by Fig. 6, the error decreases as k_{out}, or equivalently r_{out}, decreases (it is also confirmed as $\partial s/\partial r_{out} = (1/\min\{r_{in}, 2\})\partial\hat{C}/\partial r_{out} > 0$).

Part (ii) means that, if $r_{in} \geq r_{out}$, the error $s(r)$ is bounded from above by $s(2, 2) \approx 0.618$. Thus, under this simple condition, the relative error does not exceed approximately 61.8%.

Part (iii) shows that, by imposing the additional lower bound $r_{in} \geq 2\lambda$ with $\lambda \geq 1$, the error can be bounded by an upper bound δ_λ that decreases as λ increases. Under the conditions of part (iii), the approximation is given by $\min\{r_{in}, 2\} = 2$. Therefore, the absolute difference between $|\hat{C}|$ and the approximation value 2 is at most δ_λ times the approximation value. The upper bound δ_λ decreases from $s(2, 2) \approx 0.618$ at $\lambda = 1$, corresponding to $r_{in} = 2$, and approaches 0.5 in the limit $\lambda \to \infty$. Thus, in this limit, the absolute difference between $|\hat{C}|$ and the approximation value 2 is bounded above by one

half of the approximation value. The implications of part (iii) are discussed further in the remainder of this subsection.

3. *Possibility of Determining $|C|$ Solely from k_{tra}*

We now consider the unscaled parameter $|C|$ itself under the conditions of part (iii), namely, $r_{in} \geq r_{out}$ and $r_{in} \geq 2$. A lower bound for $|C|$ follows from the result of part (iii), whereas an upper bound follows from Eq. (62). Thus, we obtain

$$2k_{tra} > |C| \geq s_\lambda \times 2k_{tra}. \tag{70}$$

Here, the factor $s_\lambda \equiv 1 - \delta_\lambda$ increases with λ and takes values in the range

$$0.382 \approx \frac{3-\sqrt{5}}{2} \leq s_\lambda < \frac{1}{2}.$$

Thus, $|C|$ is smaller than the approximation value $2k_{tra}$, but is at least s_λ times this value.

Let us now recall the discussion in Sec. VI B 2. Under the conditions given by Eqs. (49) and (50), mode C can be regarded as the mode that characterizes the permeation behavior, and $|C|$ can be used to characterize the permeation rate. Among the conditions in Eq. (49), consider

$$r_{in} \geq 3 \quad (\Leftrightarrow k_{in} \geq 3k_{tra})\,. \tag{71}$$

Since this condition is consistent with part (iii) by taking $\lambda = 1.5$, we have

$$2k_{tra} > |C| \geq s_{1.5} \times 2k_{tra} \approx 0.419 \times 2k_{tra}. \tag{72}$$

That is, $|C|$ is at least approximately 40% of $2k_{tra}$, while remaining smaller than $2k_{tra}$. Thus, when only the order of magnitude of $|C|$ is of interest, $|C|$ may be approximated by $2k_{tra}$:

$$|C| \approx 2k_{tra}. \tag{73}$$

Therefore, if Eq. (71) and

$$r_{in} \geq r_{out} \quad (\Leftrightarrow k_{in} \geq k_{out}) \tag{74}$$

can be assumed, and if the initial conditions can be chosen according to Eq. (50), the order of magnitude of permeation rate $|C|$ can be estimated solely from k_{tra} by the approximation

$|C| \approx 2k_{tra}$. In particular, knowledge of the rate constant k_{tra} for the transition from the first lipid phase to the second lipid phase is sufficient to estimate the order of magnitude of the permeation rate. This result may contribute to reducing the computational or experimental cost of predicting the permeation rate. For example, in MD simulations, focusing on the determination of k_{tra} alone could significantly reduce the corresponding computational effort. A related result was reported in Ref. [11], in which the flip process, involving passage through the center of the membrane, was found to be a rate-limiting step in membrane permeation for most peptides considered in the calculations.

Design Guidelines–. From the perspective of designing target molecules introduced into the membrane, the above results also provide a basis for establishing design guidelines centered on increasing k_{tra}. When the conditions of the environment, consisting of water molecules and membrane molecules, are fixed, examples of possible design guidelines for the target molecules are as follows.

1. Increase k_{in} so that the condition Eq. (74) is satisfied. When dealing with a group of molecules for which this condition is satisfied by default, the design can focus primarily on increasing k_{tra}.

2. Considering Eq. (70), we can use k_{tra} as a reference for setting the target order of magnitude of $|C|$. Thus, One may first design a target order of magnitude for $|C|$ and then design molecules for which k_{tra} reaches the corresponding value. After this target has been achieved, if k_{tra} is maintained while k_{in} is further increased (or k_{out} is decreased), $|C|$ can in principle be increased toward $2k_{tra}$. However, the possible increase is limited to less than a factor of two relative to k_{tra}, so the priority given to further modifications of k_{in} or k_{out} should be considered carefully.

The conditions given by Eqs. (71) and (74), which underlie the cost reduction and molecular design guidelines discussed above, have been satisfied, at least based on our experience with the MD calculations performed so far. A specific example is presented in the next section.

The other condition considered in Sec. VI B 2, Eq. (50), is different in nature. It concerns how the target molecules are initially distributed, rather than an intrinsic property of each molecule. Therefore, this condition is independent of the molecular properties obtained from the MD simulations and can be fully controlled within the master-equation approach.

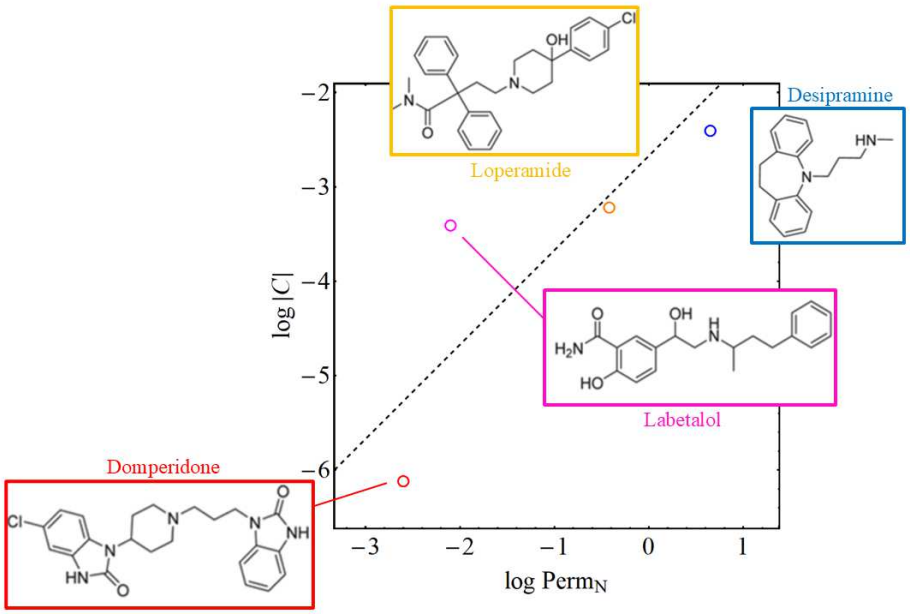


FIG. 8: Permeation coefficient $\mathrm{Perm_N}$ (cm $\mathrm{s^{-1}}$) [40] plotted against $|C|$ ($\mathrm{ns^{-1}}$), calculated from the rate parameters obtained from WE simulations. The dashed line represents a line with a slope of 1 and a y-intercept of $\langle \log(c_0) \rangle$, where $c_0(i) = |C|(i)/\mathrm{Perm_N}(i)$ for each molecule i.

VIII. MOLECULAR SIMULATION

A. Simulation Objectives

We performed molecular simulations of a target system, which consists of a membrane system, its surrounding environment, and the molecules of interest, to examine the following two issues concerning the rate parameters:

(A) whether the sufficient condition given by Eq. (71) is satisfied for the molecules studied, so that $|C|$ can be regarded as the permeation rate;

(B) whether, in addition to Eq. (71), the condition given by Eq. (74) is satisfied for these molecules, and how accurately $|C|$ can be approximated by $2k_{tra}$.

We simulated the permeation of four small molecule compounds, Desipramine, Loperamide, Labetalol, and Domperidone, from state 1 to state 4 (Fig. 8). To determine the rate parameters k_{in}, k_{out}, and k_{tra}, we performed weighted-ensemble (WE) simulations using multiple MD trajectories.

B. Simulation Conditions

a. MD Simulations: The MD simulation box containing the target system was rectangular, with dimensions of 58.5 Å × 58.5 Å × 110 Å. The membrane region, consisting of sites 2 and 3, spans approximately 40 Å along the z-axis. The membrane system consisted of 72 POPC molecules and 48 cholesterol molecules, corresponding to a cholesterol concentration of 40 mol%. The surrounding environment, defining sites 1 and 4, contained $\sim$ 3600 TIP3P water molecules [34] in each state, together with 19 K^+ and 19 Cl^- ions to give a KCl concentration of 0.15 M. The simulation system was constructed using the CHARMM-GUI Membrane Builder [35]. A snapshot of all molecules is shown in Fig. S6.

The AMBER Lipid14 force field was used for POPC and cholesterol [36, 37]. The force-field parameters of the four compounds were obtained from the general AMBER force field 2 (GAFF2) [38], supplemented by quantum chemical calculations at the Hartree–Fock level with the 6-31G** basis set using Gaussian 16 [39]. After the system was equilibrated in the NPT ensemble at the temperature $T = 300$ K and pressure $P = 1$ atm, production runs were performed in the NVT ensemble at $T = 300$ K. All MD simulations were conducted using AMBER 20.

b. WE Simulations: The WE simulations using the original Huber–Kim algorithm [28] were performed to sample the pathways of the membrane permeation process and to calculate the kinetic rate constants. The position of the center of mass of the compound along the membrane normal, z, was used as the collective variable, with $z = 0$ corresponding to the membrane center. The WE simulations were performed separately for three processes: entry into the membrane (corresponding to k_{in}), flip-flop across the membrane center (corresponding to k_{tra}), and exit from the membrane (corresponding to k_{out}). In each WE simulation, 16 walkers were maintained in each bin, and the resampling time interval was set to 20 ps. The progress coordinate ranged from $z = 45$ to 8 Å for entry, from 14 to -14 Å for flip-flop, and from -8 to -45 Å for exit, and was divided into 9, 16, and 21 bins, respectively. Each WE simulation was run for 200–600 iterations (4–12 ns), which provided estimates of the rate constants.

TABLE III: Rate parameters k_{in}, k_{out}, k_{tra} (ns^{-1}) obtained from the molecular simulations, resulting $|C|$ (ns^{-1}) according to Eq. (3c), and experimental values of the permeation coefficient $\mathrm{Perm_N}$ (cm s^{-1}) [40]; r_{in} and r_{out} are nondimensional scaled rate parameters defined by Eq. (33).

	k_{in}	k_{out}	k_{tra}	$\lvert C\rvert$	r_{in}	r_{out}	$\mathrm{logPerm_N}$
Desipramine	2.0E−02	3.2E−04	2.0E−03	4.0E−03	1.0E+01	1.6E−01	6.5E−01
Loperamide	2.4E−03	5.1E−05	3.1E−04	6.0E−04	7.7E+00	1.6E−01	-4.2E−01
Labetalol	3.1E−03	2.1E−04	2.1E−04	3.9E−04	1.5E+01	1.0E+00	-2.1E+00
Domperidone	2.5E−03	1.3E−04	4.0E−07	7.6E−07	6.3E+03	3.3E+02	-2.6E+00

C. Calculation Results

Table III summarizes the rate parameters k_{in}, k_{out}, and k_{tra} obtained from the molecular simulations, together with $|C|$ and the experimental values of the permeation coefficient [40]. From the fastest-permeating molecule, Desipramine, to the slowest-permeating molecule, Domperidone, the experimental values span approximately four orders of magnitude. To compare the calculated $|C|$, which has the dimension of an inverse time, with the experimental permeation coefficient $\mathrm{Perm_N}$, which has that of a velocity, we relate them through a proportionality constant $c_0(i) = |C|(i)/\mathrm{Perm_N}(i)$ of dimension [1/length] for each molecule i. As shown in Fig. 8, $|C|$ and $\mathrm{Perm_N}$ lie approximately along a line of unit slope in the log-log plot, so that $c_0(i)$ is nearly constant across molecules; this supports both the identification of $|C|$ as the permeation rate (Eq. (51)) and its proportionality to the permeation coefficient.

Thus, the calculated results provide a sound basis for assessing the two issues raised in Sec. VIII A. We observe in Table III that

(A) all four molecules satisfy the condition given by Eq. (71). Therefore, $|C|$ can be regarded as the permeation rate for these molecules;

(B) the condition given by Eq. (74) is satisfied for all four molecules. Furthermore, the relative error of this approximation, namely the left-hand side of Eq. (67), is at most 7.1%, for Labetalol. Thus, the approximation $|C| \approx 2k_{tra}$ provides a reasonably accurate estimate of $|C|$ for all four molecules.

As shown in Table III, r_{in} ranges from 7.7 for Loperamide, the smallest value among the four molecules, to 6.3×10^3 for Domperidone, the largest value. For Domperidone, this

large value of r_{in} does not result from an unusually large k_{in} compared with the other molecules. Rather, k_{tra} is three to four orders of magnitude smaller than that of the other molecules. This small value of k_{tra} is therefore a major factor limiting the permeation rate of Domperidone. In other words, the transition from the first to the second lipid phase is the rate-limiting process for membrane permeation of Domperidone. Thus, k_{tra} characterizes the permeation behavior in this case. This is consistent with the approximation $|C| \approx 2k_{tra}$.

These results confirm, for the molecular systems examined here, that the theoretically derived conditions given by Eqs. (71) and (74) are satisfied. They also demonstrate that the approximation of $|C|$ derived from these conditions provides a relative accuracy of better than 7.1% for the four molecules.

IX. DISCUSSION

A. On the Master Equation Approach

The theoretical analysis of membrane permeation based on the master equation approach presented above has shown that the permeation rate can be characterized by $|C|$ obtained from Eq. (3c) by estimating the three rate parameters k_{in}, k_{out}, and k_{tra}. However, to regard $|C|$ as the permeation rate, the conditions given by Eq. (49) must first be verified. Furthermore, we have identified the conditions given by Eqs. (71) and (74) under which $|C|$ can be approximated by $2k_{tra}$. Such a detailed theoretical analysis is possible because the master equation is sufficiently simple.

From a practical perspective, a second advantage of the master equation approach is the reduction of computational cost. Instead of performing an MD simulation of the entire membrane permeation process as a single long trajectory in configuration space, the process can be divided into three subprocesses, which can then be simulated independently. This makes it possible to substantially reduce the computational cost required for sampling the relevant states. As described in Sec. VIII, we performed each of these subprocesses efficiently using WE simulations.

A third interesting aspect of the master equation approach is that it enables the time evolution of a population of molecules to be predicted. Specifically, for a population of molecules undergoing membrane permeation, the time evolution of the number of molecules

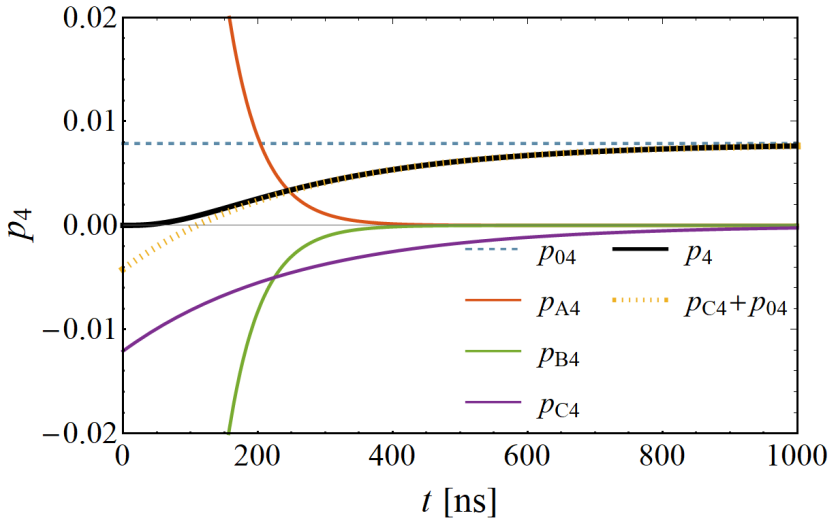


FIG. 9: For Desipramine, shown the time evolutions of the fourth component of the solution, $p_4(t)$, and the fourth components of modes, $p_{04}(t)$ (mode 0; dashed line), $p_{A4}(t)$ (mode A), $p_{B4}(t)$ (mode B), $p_{C4}(t)$ (mode C), and the sum $p_{C4}(t) + p_{04}(t)$ (dotted line), for the initial condition $\mathbf{p}(0) = (1, 0, 0, 0)^T$ and the rate parameters in Table III.

that have permeated the membrane and reached the intracellular region can be represented by $p_4(t)$, from $t = 0$ until the stationary state is reached. If desired, the time evolution of the number of molecules trapped within the membrane can also be examined from $p_2(t)$ and $p_3(t)$. It is generally difficult to observe the permeation of multiple target molecules using conventional MD simulations. In addition, the master equation approach makes it possible to examine and compare the time evolution of the molecular population under different initial conditions, namely, different fractions of molecules occupying the respective states at the initial time.

In this subsection, we discuss this third aspect in more detail. Specifically, we examine the time evolution of state 4 predicted by the master equation using the rate parameters obtained from the WE simulations described in Sec. VIII (Table III). Figure 9 shows $p_4(t)$ for Desipramine under the initial condition given by Eq. (15), together with the time evolution of the individual modes. The corresponding results for the other molecules are shown in Fig. S7.

The convergence of $p_4(t)$ toward its stationary value becomes faster in the order of the

permeation rates, Desipramine, Loperamide, Labetalol, and Domperidone. In particular, for Domperidone, the convergence is very slow, and $p_4(t)$ approaches its stationary value so gradually that a smooth initial rise is hardly observed.

1. Comparison of the Modes

Figure 9 shows that mode C indeed traces the exact solution better than the other modes. Although some deviations can be observed at early times, roughly for $t < 100$, the mode-C approximation agrees very well with the exact solution thereafter. As time increases, mode $C + 0$ converges to the stationary value q_∞. In contrast, although modes A and B individually have relatively large amplitudes at early times, they tend to cancel each other. Each of these modes decays exponentially toward zero more rapidly than mode $C + 0$. A detailed discussion of this cancellation is provided in the Supplementary Material (Fig. S7).

2. Dependence on the Initial Conditions

Supplementary Fig. S8 shows the dependence of $p_4(t)$ and the each mode on the initial conditions (a, b, c) for Desipramine. While keeping the initial probability in state 3 equal to zero (viz., $c = 0$), decreasing a and correspondingly increasing b has little effect on the behavior of $p_4(t)$ (Fig. S8(a)).

In contrast, when $c > 0$, while its long-time behavior remains qualitatively similar, the initial rise of $p_4(t)$ becomes relatively steep (Figs. S8(b)–(d)). Mathematically, this rise follows from the fact that the derivative of p_4 at $t = 0$ is positive: $\mathrm{D}p_4(0) = k_{out}c > 0$, as follows from Eqs. (1) and (2). Physically, this behavior can be understood as follows. Because some target molecules are already present in the membrane (state 3) at $t = 0$, molecules can reach state 4 without first undergoing the transitions $1 \to 2 \to 3$. These molecules can therefore leave state 3 rapidly, with an amount $k_{out}c$ leaving per unit time. Consequently, the initial permeation appears to be accelerated. Thus, this initial increase does not represent the essential permeation process in which molecules enter the membrane from the outside and subsequently leave it on the opposite side. A related distinction between the initial rise in the receiver-side concentration and the permeation process has also been discussed by Ghaemi *et al.* [18].

We further examined various initial conditions satisfying $b \geq c > 0$ under condition (40) for which $a \geq a_{\min} = 0.5$ in the current cases. The behavior of $p_4(t)$ was found to vary only modestly among these initial conditions (Fig. S9). This indicates that the overall permeation behavior is relatively robust to the presence of molecules initially distributed within the membrane. We also found that, compared with the case $c = 0$, mode $C+0$ tends to provide a better approximation to the exact solution (Fig. S8). Thus, the presence of target molecules within the membrane at the initial time can improve the approximation of the exact solution by mode C compared with the case in which no target molecules are initially present inside the membrane. This tendency can be understood mathematically from the initial slopes. When case (v) or case (vii) applies, both the exact solution and mode C have a positive initial slope: $\mathrm{D}p_4(0) = k_{out}c > 0$ and $\mathrm{D}p_{C4}(0) = Cc_C > 0$. Thus, the initial increase of mode C is qualitatively consistent with that of the exact solution. For all four molecules, every initial condition satisfying condition (50), namely $a \geq a_{\min} = 0.5$ in these cases, belongs to case (vii) (see Fig. S10).

B. Analysis of the Stationary Population in State 4

So far, we have focused on the permeation rate characterized by mode C, or on its relative advantage over mode B. Here, we reconsider the role of mode 0, which has served as an offset in comparing these modes. The quantity q_∞ associated with mode 0 is a function only of the rate parameters k and is therefore an intrinsic property of the system that is independent of the initial conditions. Specifically, q_∞ is the stationary value of $p_4(t)$, that is, the value approached by $p_4(t)$ as $t \to \infty$ for any initial condition. As discussed in Sec. III B 2, it is given by

$$q_\infty = \lim_{t\to\infty} p_4(t) = c_0 k_{out} = \frac{1}{2(k_{in}/k_{out} + 1)}. \tag{75}$$

Although q_∞ does not generally represent the amount of molecules newly permeating from the initial state, it characterizes the stationary fraction of molecules occupying state 4. In particular, for the initial condition $\mathbf{p}(0) = (1, 0, 0, 0)^{\mathrm{T}}$, it represents the fraction of the initially external molecular population that occupies state 4 in the long-time limit.

While we have so far focused on the rate of permeation as a characteristic of permeation behavior, the stationary population in state 4 may also be important in certain applications. For example, depending on the purpose of an application, a larger fraction of molecules

reaching and remaining in state 4 may be desirable. In such cases, the dependence of q_∞ on the rate parameters k becomes relevant. This is also related to the choice of rate parameters for increasing the permeation rate $|C|$, discussed in Sec. VII B. We examine this relationship below.

1. Design Strategies Based on the Permeation Rate and Stationary Population

The permeation rate characterized by $|C|$ and the stationary population in state 4, q_∞, have different dependences on the rate parameters k_{in}, k_{out}, and k_{tra}. This difference has important implications for molecular design.

As discussed in Sec. VII B, increasing k_{in} and k_{tra} or decreasing k_{out} is effective for increasing $|C|$. On the other hand, Eq. (75) shows that q_∞ increases with increasing k_{out} and decreases with increasing k_{in}, while it is independent of k_{tra}. The possible range of q_∞ is

$$0 < q_\infty < \frac{1}{2}. \tag{76}$$

Thus, there is a trade-off between increasing $|C|$ and increasing q_∞ through the adjustment of k_{in} and k_{out}. In contrast, increasing k_{tra} can increase $|C|$ without changing q_∞.

These relationships lead to the following design considerations:

1. **Increasing the permeation rate:** Increasing k_{in} and k_{tra} or decreasing k_{out} is effective for increasing $|C|$.

2. **Increasing the stationary population in state 4:** Increasing the ratio k_{out}/k_{in} is effective for increasing q_∞.

Consequently, increasing k_{in} or decreasing k_{out} to enhance the permeation rate may reduce the stationary population in state 4. This trade-off should be taken into account when selecting the rate parameters for a given application.

X. CONCLUSION

In this study, we described the passive permeation of molecules across a membrane in an aqueous and lipid-bilayer environment using a four-state master equation. The four states represent the aqueous phase outside the membrane, the first and second lipid phases within

the membrane, and the aqueous phase on the opposite side of the membrane. Transitions between these states are characterized by three rate parameters, k_{in}, k_{out}, and k_{tra}. In an n-state master equation, the characteristic equation for the eigenvalues is an algebraic equation of degree n, which can be solved algebraically for $n \leq 4$. This property allowed us to obtain explicit expressions for the eigenvalues in the present four-state model and to quantitatively analyze the dependence of the permeation rate on the rate parameters. For models with five or more states, the range of possible applications can be extended, but explicit algebraic expressions for the eigenvalues are generally no longer available, necessitating analytical or numerical approaches. Another possible direction is to explore alternative ways of characterizing the dynamics without relying on explicit eigenvalue expressions, such as the intrinsic timing function [41], although its potential to provide useful insights into membrane permeation remains to be investigated.

In this study, we demonstrated that the eigenvalue C with the smallest absolute value does not necessarily characterize membrane permeation. Depending on the initial conditions and rate parameters, mode B can provide a better description of the permeation behavior than mode C. However, the exceptional parameter regions were found to be localized within limited regions of the r-space. Based on this finding, we derived simple and practically applicable sufficient conditions under which mode C can be regarded as the mode characterizing permeation and $|C|$ can be used as an indicator of the permeation rate. Specifically, these conditions consist of conditions on the rate parameters, given by Eq. (71) or, more generally, Eq. (49), and a condition on the initial conditions, given by Eq. (50).

Furthermore, using the explicit algebraic expression for $|C|$, we showed that, in the parameter region satisfying Eq. (74), $|C|$ can be approximated by the simple expression $2k_{tra}$. This result indicates that, within this parameter region, the transition rate between the two lipid phases within the membrane plays a major role in characterizing the permeation rate. It also suggests that the order of magnitude of the permeation rate can be estimated from k_{tra} alone, providing a basis for reducing the computational or experimental effort required for its evaluation and for developing molecular design guidelines. We also analyzed the stationary population in state 4, q_∞, and showed that its dependence on the rate parameters differs from that of the permeation rate $|C|$. This difference implies that both quantities may need to be considered when designing molecules for specific applications.

To examine the applicability of these theoretical results, we performed molecular simula-

tions of membrane permeation for four small molecules. For all four molecules, the condition required for regarding $|C|$ as the permeation rate was satisfied. Furthermore, the additional condition required for the approximation $|C| \approx 2k_{tra}$ was also satisfied, and the relative error of this approximation was at most 7.1%. The calculated permeation rates were also consistent with the corresponding experimental values. These results demonstrate the applicability of the both theoretically derived conditions and approximation to the molecular systems examined in this study.

In summary, by combining mathematical analysis based on the master equation with molecular simulations, we established relationships between the rate parameters and membrane permeation behavior and derived guidelines that may be useful for molecular design. Although the master equation alone cannot directly describe how changes in molecular structure affect membrane permeation, such effects can be investigated through detailed molecular simulations. By incorporating information obtained from these simulations into the rate parameters of the master equation, the present approach provides a means of connecting molecular-level properties with the kinetic characteristics of membrane permeation. Future work will further investigate how molecular structure and membrane environment affect the individual rate parameters, with the aim of developing this approach for predicting membrane permeability and guiding molecular design.

Supplementary Material

The article contains a supplementary file that provides supplementary information to the main text.

Acknowledgment

IF would like to thank Yoshifumi Fukunishi for insightful discussions on membrane permeation, which highlighted the challenges and fascinating aspects of this subject. Part of the molecular simulations was conducted on the Research Center for Computational Science, Okazaki, Japan, and on the HPCI system provided by Kyushu University through the HPCI System Research Project (hp250041 and hp260075).

Declarations

Conflict of interest We declare that we have no conflict of interest.

Data availability

The authors declare that the data supporting the findings of this study are available within the paper and its Supplementary Material. Should any raw data files be needed in another format they are available from the corresponding author upon reasonable request.

Appendix A: Proof of Eq. (5)

First of all, since D can be represented as

$$D = (k_{in} + k_{out})^2 + 4k_{tra}(k_{out} - k_{in}) + 4k_{tra}^2 \tag{77a}$$

$$= (k_{in} - 2k_{tra})^2 + k_{out}^2 + 2k_{in}k_{out} + 4k_{out}k_{tra} \tag{77b}$$

$$> 0, \tag{77c}$$

$\sqrt{D}$ is a strictly positive real number.

Next, $C < 0$ can be shown from

$$(k_{in} + k_{out} + 2k_{tra})^2 - D = 8k_{in}k_{tra} > 0,$$

which serves to compare the magnitudes of the two factors of C such that

$$\sqrt{D} < k_{in} + k_{out} + 2k_{tra}. \tag{78}$$

To show $B < A < C$, observe that

$$\begin{aligned} 2(C - A) &= -(k_{in} + k_{out} + 2k_{tra}) + \sqrt{D} + 2(k_{in} + k_{out}) \\ &= \sqrt{D} + (k_{in} + k_{out} - 2k_{tra}) \\ 2(A - B) &= -2(k_{in} + k_{out}) + (k_{in} + k_{out} + 2k_{tra}) + \sqrt{D} \\ &= \sqrt{D} - (k_{in} + k_{out} - 2k_{tra}). \end{aligned}$$

Thus, relationships $C - A > 0$ and $A - B > 0$ follows from

$$\sqrt{D} > |k_{in} + k_{out} - 2k_{tra}|, \tag{79}$$

which can be shown by

$$\begin{aligned} D - (k_{in} + k_{out} - 2k_{tra})^2 &= \{(k_{in} + k_{out})^2 + 4k_{tra}(k_{in} + k_{out}) + 4k_{tra}^2 - 8k_{in}k_{tra}\} \\ &\quad - \{(k_{in} + k_{out})^2 - 4k_{tra}(k_{in} + k_{out}) + 4k_{tra}^2\} \\ &= 8k_{out}k_{tra} > 0. \end{aligned}$$

Combining these results justifies Eq. (5).

Appendix B: Proof of the results in Table I

Note that the denominators in the expressions for coefficients c_A, c_B, c_C in Eq. (31) are all positive. Therefore, the signs of the coefficients are determined by the signs of their respective numerators.

Proof of (i). Setting $t = 0$ in Eq. (39) gives

$$c_A + c_B + c_C = -c_0 k_{out}.$$

By Eq. (31a), the right-hand side is negative. On the other hand, if $c_A \geq 0, c_B \geq 0, c_C \geq 0$, the left-hand side is nonnegative. Therefore, this is a contradiction. □

Proof of (ii-1). It follows from Eqs. (31c)–(31d) that $c_B > 0, c_C \geq 0$ implies

$$a\sqrt{D} < G \leq -a\sqrt{D}.$$

On the other hand, since $a \geq 0$,

$$a\sqrt{D} \geq -a\sqrt{D}.$$

Therefore, this is a contradiction. □

Proof of (ii-2). If $c_B = 0, c_C > 0$, then

$$a\sqrt{D} = G < -a\sqrt{D}$$

must hold. On the other hand, since $a \geq 0$, this is a contradiction. □

Proof of (ii-3). If $c_B = 0, c_C = 0$, then

$$G = a\sqrt{D} = -a\sqrt{D}.$$

Since $a \geq 0$ and $D > 0$, this implies $a = 0$ and hence $G = 0$. Conversely, if $a = G = 0$, then $c_B = c_C = 0$. Therefore,

$$\begin{aligned} c_B = 0, c_C = 0 &\Leftrightarrow a = G = 0 \\ &\Rightarrow c_A < 0. \end{aligned}$$

Thus, case (ii-3) $\Leftrightarrow c_B = 0, c_C = 0$. Furthermore, from Eq. (30),

$$a = G = 0 \Leftrightarrow a = 0, \quad b = c = \frac{1}{2} \tag{80}$$

Indeed, under $a = 0$, the condition $G = 0$ implies $b = c$, and condition (29) then gives $b = c = 1/2$. The converse is immediate. Therefore, case (ii-3) occurs only at the single point

$$a = 0, \quad b = c = \frac{1}{2}, \tag{81}$$

which is a set of measure zero in Ω. $\square$

Proof of (iii)–(viii). To show that cases (iii)–(viii) can occur, it is sufficient to provide a specific example for each case. We provide examples for cases (iv)–(viii) in Example A and for case (iii) in Example B.

Example A (uniform parameter case): Consider the case in which the three parameters k_{in}, k_{out}, k_{tra} have the same value $\bar{k}$. For any $\bar{k} > 0$, we then have

$$\sqrt{D} = 2\sqrt{2}\bar{k},$$
$$G = 2\bar{k}(b - c + a) = 2\bar{k}(1 - 2c).$$

Therefore,

$$\text{numerator of } c_A = (2a - 1)\bar{k},$$
$$\text{numerator of } c_B = 2\bar{k}(1 - (2c + \sqrt{2}a)),$$
$$\text{numerator of } c_C = -2\bar{k}(1 - (2c - \sqrt{2}a)).$$

Under condition (29), each of these quantities can be positive, negative, or zero. As shown by the different colored regions in Fig. 3, cases (iv)–(viii) are indeed realized. In particular, the sign pattern can be confirmed by selecting any representative point in each colored region.

The lower triangular region in Fig. 3 corresponds to the target region Ω. Therefore, case (iii) does not occur in the uniform parameter case. However, case (iii) can occur if the vertical boundary line in Fig. 3 are shifted to the left. In fact, it is sufficient to consider $k_{in} > k_{out}$. We give such an example in Example B.

Example B ($k_{in} > k_{out}$): Consider the parameters

$$k_{in} = 5\bar{k}, \quad k_{tra} = \bar{k}, \quad k_{out} = \bar{k}. \tag{82}$$

Here, $\bar{k} > 0$ is an arbitrary scale factor. In this case, case (iii), which is excluded in the uniform parameter case, appears in the green region shown in Fig. S2(a). The corresponding sign pattern can be confirmed by selecting any representative point in this region.

□

For comparison, an example with $k_{in} < k_{out}$ is also shown in Fig. S2(b).

Appendix C: Proof of Proposition 2

From the assumption, Eq. (41) holds. Now, Eqs. (35a) and (37) indicate

$$\begin{aligned} & c_A \geq 0 \\ & \Leftrightarrow (r_{in} + r_{out})a - r_{out} \geq 0 \\ & \Leftrightarrow a \geq \frac{1}{r_{in}/r_{out} + 1}. \end{aligned} \tag{83}$$

Thus, Eq. (41(b)) leads to $c_A \geq 0$.

Putting

$$h(r) := r_{in} + r_{out} - 2 - \sqrt{(r_{in} + r_{out} + 2)^2 - 8r_{in}}, \tag{84}$$

we represent the numerator of $\hat{c}_C$ (Eq. (35c)) by

$$-\hat{G}(a, c; r) - a\sqrt{\hat{D}(r)} = h(r)a + 4r_{out}c - 2r_{out}. \tag{85}$$

This means that the subset of Ω such that $\hat{c}_C$, so that c_C, is nonnegative consists of points $(a, c) \in \Omega$ such that

$$c \geq -\frac{h(r)}{4r_{out}}a + \frac{1}{2} =: h'(r)a + \frac{1}{2}. \tag{86}$$

Multiplying Eq. (84) by k_{tra} yields

$$k_{tra}h(r) = k_{in} + k_{out} - 2k_{tra} - \sqrt{D} < 0, \tag{87}$$

where the inequality comes from Eq. (79). Thus, for any $r \in \mathbb{R}^2_+$, it holds that

$$h'(r) > 0. \tag{88}$$

From Eq. (41(a)), $a \geq \frac{1}{2}$ is valid. Hence, Eqs. (86) and (88) along with $a > 0$ yield

$$\begin{aligned} & c_C \geq 0 \\ & \Leftrightarrow c \geq h'(r)a + \frac{1}{2} \\ & \Rightarrow c > \frac{1}{2}. \end{aligned} \tag{89}$$

From this result and from the fact that $c = 1 - a - b \leq \frac{1}{2} - b \leq \frac{1}{2}$, we have $c_C < 0$.

These results complete the proof. □

For comparison, we have

$$c_B \geq 0 \Leftrightarrow c \leq g'(r)a + \frac{1}{2}, \tag{90}$$

where

$$g'(r) := \frac{1}{4r_{out}} \left[-r_{in} - r_{out} + 2 - \sqrt{\hat{D}(r)} \right].$$

Appendix D: Proof of Equations in Sec. VII

We give proofs of equations presented in Sec. VII, which are properties concerning C defined by Eq. (3c). Starting from proofs of the *limit formulas in Table II*, we immediately observe that

$$\begin{aligned} \lim_{k_{out} \to 0} C &= \frac{1}{2} \left[-(k_{in} + 2k_{tra}) + |k_{in} - 2k_{tra}| \right] \\ &= -\min\{k_{in}, 2k_{tra}\} \end{aligned} \tag{91}$$

and that $\lim_{k_{in} \to 0} C = \lim_{k_{tra} \to \infty} C = 0$. Rationalizing C, we have

$$C = \frac{-4k_{in}k_{tra}}{\sqrt{D} + k_{in} + k_{out} + 2k_{tra}},$$

where the division of the numerator and denominator by $k_{in} > 0$ yields

$$\lim_{k_{in} \to \infty} C = \frac{-4k_{tra}}{2} = -2k_{tra}. \tag{92}$$

The remaining limits can be similarly obtained such that

$$\lim_{k_{tra} \to \infty} C = -k_{in}, \tag{93a}$$

$$\lim_{k_{out} \to \infty} C = 0. \tag{93b}$$

□

Eqs. (53), (57), and (59) follow from Eqs. (93a) (92), and (91), respectively. □

Eq. (52) can be derived from the first-order approximation of $\sqrt{D}$ with respect to k_{tra}, by assuming $k_{tra} \ll k_{in}, k_{out}$ and using Eq. (77a), such that

$$\begin{aligned}\sqrt{D} &= \sqrt{(k_{in}+k_{out})^2 + 4k_{tra}(k_{out}-k_{in}) + 4k_{tra}^2} \\ &\approx \sqrt{(k_{in}+k_{out})^2\left(1+\frac{4k_{tra}(k_{out}-k_{in})}{(k_{in}+k_{out})^2}\right)} \\ &\approx (k_{in}+k_{out})\left(1+\frac{1}{2}\frac{4k_{tra}(k_{out}-k_{in})}{(k_{in}+k_{out})^2}\right).\end{aligned}$$

Substituting this into C yields

$$\begin{aligned}C &\approx \frac{1}{2}\left[-(k_{in}+k_{out}) - 2k_{tra} + (k_{in}+k_{out}) + \frac{2k_{tra}(k_{out}-k_{in})}{k_{in}+k_{out}}\right] \\ &= -\frac{2k_{in}}{k_{in}+k_{out}}k_{tra}.\end{aligned} \tag{94}$$

□

Eq. (55) comes from observation of Eqs. (3c) and (4) such that C is invariant under the transformation

$$\varphi : k = (k_{in}, k_{out}, k_{tra}) \mapsto \left(2k_{tra}, k_{out}, \tfrac{1}{2}k_{in}\right). \tag{95}$$

Namely,

$$C(k') = C(\varphi(k)) = C(k) \tag{96}$$

with

$$\varphi(k) =: k' = (k'_{in}, k'_{out}, k'_{tra}) = \left(2k_{tra}, k_{out}, \tfrac{1}{2}k_{in}\right).$$

□

Eq. (56) can be derived from Eq. (94) and Eq. (96), for which the assumption $k_{in} \ll k_{out}, k_{tra}$ corresponds to $k'_{tra} \ll k'_{out}, k'_{in}$, such that

$$\begin{aligned}C(k) &= C(k') \\ &\approx -\frac{2k'_{in}}{k'_{in}+k'_{out}}k'_{tra} \\ &= -\frac{2k_{tra}}{k_{out}+2k_{tra}}k_{in}.\end{aligned}$$

□

Eq. (60) can be shown, under the assumption $k_{out} \gg k_{in}, k_{tra}$, such that

$$\begin{aligned}\sqrt{D} &= (k_{in} + k_{out} + 2k_{tra}) \left[1 - \frac{8k_{in}k_{tra}}{(k_{in} + k_{out} + 2k_{tra})^2}\right]^{1/2} \\ &\approx (k_{in} + k_{out} + 2k_{tra}) \left[1 - \frac{4k_{in}k_{tra}}{(k_{in} + k_{out} + 2k_{tra})^2}\right]\end{aligned}$$

whose substitution into C yields

$$C \approx -\frac{2k_{in}k_{tra}}{k_{in} + k_{out} + 2k_{tra}} \approx -\frac{2k_{in}k_{tra}}{k_{out}}.$$

□

Eq. (54) is shown through Eq. (4) such that

$$\begin{aligned}\frac{\partial C}{\partial k_{tra}} &= -1 + \tfrac{1}{4} D^{-\frac{1}{2}} 4(-k_{in} + k_{out} + 2k_{tra}) \\ &= D^{-\frac{1}{2}}[(-k_{in} + k_{out} + 2k_{tra}) - D^{\frac{1}{2}}].\end{aligned}$$

Here, since

$$\begin{aligned}&D - (-k_{in} + k_{out} + 2k_{tra})^2 \\ &= (k_{out} + 2k_{tra} + k_{in})^2 - (k_{out} + 2k_{tra} - k_{in})^2 - 8k_{in}k_{tra} \\ &= 4k_{in}k_{out} > 0,\end{aligned}$$

it holds that

$$\sqrt{D} > |-k_{in} + k_{out} + 2k_{tra}| \geq -k_{in} + k_{out} + 2k_{tra}, \tag{97}$$

implying

$$-\frac{\partial |C|}{\partial k_{tra}} = \frac{\partial C}{\partial k_{tra}} < 0 \tag{98}$$

for all $k_{in}, k_{out}, k_{tra} > 0$. □

Eq. (58) is deduced from the symmetric relationship (96) and the results (98) for $k_3 \equiv k_{tra}$. That is, for any $k = (k_{in}, k_{out}, k_{tra})$, we have

$$\begin{aligned}-\frac{\partial |C|}{\partial k_{in}} &= \mathrm{D}_1 C(k) = \mathrm{D}_1 (C \circ \varphi)(k) \\ &= \mathrm{D}C(\varphi(k)) \circ (0, 0, \tfrac{1}{2}) \\ &= \tfrac{1}{2} \mathrm{D}_3 C(\varphi(k)) < 0\end{aligned}$$

for all $k_{in}, k_{out}, k_{tra} > 0$. Here D_i indicates the partial differentiation with respect to the ith variable. □

Eq. (61) is obtained such that for any $k = (k_{in}, k_{out}, k_{tra})$,

$$\begin{aligned} 2\frac{\partial C}{\partial k_{out}} &= -1 + \tfrac{1}{2} D^{-\frac{1}{2}} 2(k_{in} + k_{out} + 2k_{tra}) \\ &= D^{-\frac{1}{2}}[k_{in} + k_{out} + 2k_{tra} - D^{\frac{1}{2}}] \\ &> 0, \end{aligned}$$

where the last inequality comes from Eq. (78). □

Eq. (62) follows from Eqs. (61) and (91) such that

$$\forall k = (k_{in}, k_{out}, k_{tra}) \in \mathbb{R}^3_+,\ |C(k)| < \sup_{k_{out}>0} |C(k)| = \lim_{k_{out}\to 0} |C(k)| = \min\{k_{in}, 2k_{tra}\}.$$

□

Eq. (63) follows from the fact that $\sup|C| = \infty$, as confirmed, for example, by taking $k_{in} = k_{out} = k_{tra} =: \bar{k} \in (0, \infty)$, for which $|C| = (2 - \sqrt{2})\bar{k}$. While $|C| > 0$ is shown in Appendix A. □

Appendix E: Proof of Proposition 10

Proof of (i). First, from Eq. (62), we see

$$\begin{aligned} s(r) &= \frac{-|\hat{C}| + \min\{r_{in}, 2\}}{\min\{r_{in}, 2\}} > 0 \\ &= 1 - |\hat{C}|/\min\{r_{in}, 2\} < 1. \end{aligned}$$

Second, defining

$$d \equiv 2 - 2(1 - \delta)\min\{r_{in}, 2\} =: 2d',$$

we have

$$r_{in} + r_{out} + d > 0. \tag{99}$$

This is because if $r_{in} > 2$, then $d = 2(2\delta - 1) > -2$ and so $r_{in} + r_{out} + d > r_{in} - 2 + r_{out} > 0$; if $r_{in} \le 2$, then $r_{in} + r_{out} + d = (1 + (2\delta - 1))r_{in} + r_{out} + 2 > 2 - r_{in} + r_{out} \ge r_{out} > 0$. Thus

$$
\begin{aligned}
& s(r) \le \delta \\
& \quad \Longleftrightarrow \ \hat{C} + \min\{r_{in}, 2\} \le \min\{r_{in}, 2\} \cdot \delta \\
& \quad \Longleftrightarrow \ -(r_{in} + r_{out} + 2) + \sqrt{\hat{D}} + 2(1-\delta)\min\{r_{in}, 2\} \le 0 \\
& \quad \Longleftrightarrow \ \sqrt{\hat{D}} \le r_{in} + r_{out} + d \\
& \quad \Longleftrightarrow \ \hat{D} \le (r_{in} + r_{out} + d)^2 \ (\because \text{Eq. (99)}) \\
& \quad \Longleftrightarrow \ (2d - 4 + 8)r_{in} + (2d - 4)r_{out} + d^2 - 4 \ge 0 \\
& \quad \Longleftrightarrow \ (d' + 1)r_{in} + (d' - 1)r_{out} + d'^2 - 1 \ge 0 \\
& \quad \Longleftrightarrow \ r_{out} \le \frac{1 + d'}{1 - d'} r_{in} - (1 + d') \\
& \quad \Longleftrightarrow \ r_{out} \le (2 + (\delta - 1)\min\{r_{in}, 2\}) \left[\frac{1}{(1-\delta)\min\{r_{in}, 2\}} r_{in} - 1 \right] \\
& \quad \Longleftrightarrow \ r_{out} \le \left\{ \begin{array}{ll} (2 + (\delta - 1)r_{in}) \left[\frac{1}{1-\delta} - 1 \right] & \text{for } r_{in} \le 2 \\ 2(1 + \delta - 1) \left[\frac{1}{2(1-\delta)} r_{in} - 1 \right] & \text{for } r_{in} > 2 \end{array} \right\},
\end{aligned}
$$

which is equivalent to statement (i), where $s(r) = \delta$ holds if and only if r_{out} equals to the RHS of the last line. $\square$

Proof of (ii). It follows from Eqs. (38) and (61) that

$$\mathrm{D}_2 \hat{C}(r) = \mathrm{D}_2 C(k) > 0.$$

Thus, $r_{in} \ge r_{out}$ indicates

$$\hat{C}(r) = \hat{C}(r_{in}, r_{out}) \le \hat{C}(r_{in}, r_{in}). \tag{100}$$

Here $\hat{\hat{C}}$ defined by

$$
\begin{aligned}
\hat{\hat{C}}(r_{in}) &:= \hat{C}(r_{in}, r_{in}) \\
&= \frac{1}{2} \left(-(2r_{in} + 2) + \sqrt{\hat{D}(r_{in}, r_{in})} \right) \\
&= -(r_{in} + 1) + \sqrt{r_{in}^2 + 1}
\end{aligned} \tag{101}
$$

becomes strictly monotone decreasing, since

$$\mathrm{D}\hat{\hat{C}}(y) = \frac{y}{\sqrt{y^2 + 1}} - 1 < 0 \tag{102}$$

holds for any $y > 0$. Thus,

$$\hat{C}(r) \leq \hat{\hat{C}}(r_{in}) \leq \hat{\hat{C}}(u), \tag{103}$$

where $u \equiv \min\{r_{in}, 2\}$, so that

$$s(r) = \frac{\hat{C}(r) + u}{u} \leq \frac{\hat{\hat{C}}(u) + u}{u}.$$

Hence, in case of $r_{in} \geq 2$, it follows from $u = 2$ that

$$s(r) \leq \frac{\hat{C}(2,2) + 2}{2} = s(2,2).$$

While in case of $r_{in} < 2$, we have

$$\begin{aligned} s(r) &\leq \frac{\hat{C}(r_{in}, r_{in}) + r_{in}}{r_{in}} =: \hat{\hat{s}}(r_{in}) \\ &< \hat{\hat{s}}(2) = s(2,2), \end{aligned}$$

where the second inequality comes from

$$\begin{aligned} \mathrm{D}\hat{\hat{s}}(y) &= \frac{1}{y^2}[y\mathrm{D}\hat{\hat{C}}(y) - \hat{\hat{C}}(y)] \\ &= \frac{1}{y^2}\frac{1}{\sqrt{y^2+1}}[\sqrt{y^2+1} - 1] > 0 \end{aligned}$$

for any $y > 0$. □

Proof of (iii). Since (iii) is a special case of (ii) with $r_{in} \geq 2\lambda \geq 2$, Eqs. (102) and (103) indicate

$$\hat{C}(r) \leq \hat{\hat{C}}(r_{in}) \leq \hat{\hat{C}}(2\lambda),$$

leading to

$$s(r) = \frac{\hat{C}(r) + 2}{2} \leq \frac{\hat{\hat{C}}(2\lambda) + 2}{2}. \tag{104}$$

Eq. (101) leads the RHS of Eq. (104) to be

$$\begin{aligned} \frac{\hat{\hat{C}}(2\lambda) + 2}{2} &= s(2\lambda, 2\lambda) =: \delta_\lambda \\ &= \frac{1}{2}\left(-2\lambda + 1 + \sqrt{4\lambda^2 + 1}\right). \end{aligned}$$

Since $\lim_{y\to\infty}\hat{\hat{C}}(y) = -1$, it holds that$\lambda_{\to\infty}\delta_\lambda = 1/2$. From Eq. (102) we have $\frac{\mathrm{d}}{\mathrm{d}\lambda}\delta_\lambda = \mathrm{D}\hat{\hat{C}}(2\lambda) < 0$, indicating that $\lambda \mapsto \delta_\lambda$ is strictly monotone decreasing. In particular, $s(2,2) = \delta_1 = \frac{1}{2}\left(-1+\sqrt{5}\right)$, as claimed in (ii). □

---

[1] P. Läuger, Mechanisms of biological ion transport — carriers, channels, and pumps in artificial lipid membranes. Angew. Chem. Int. Ed. Engl. **24**, 905 (1985)

[2] S.D. Krämer, D. Lombardi, A. Primorac, A.V. Thomae, H. Wunderli-Allenspach, Lipid-bilayer permeation of drug-like compounds. Chem. Biodivers. **6**, 1900 (2009)

[3] M.P. Allen, D.J. Tildesley, *Computer Simulation of Liquids* (Oxford University Press, New York, 2002)

[4] T. Schlick, Molecular *Modeling and Simulation: An Interdisciplinary Guide* (Springer, New York, 2006)

[5] E. Awoonor-Williams, C.N. Rowley, Molecular simulation of nonfacilitated membrane permeation. Biochim. Biophys. Acta **1858**, 1672 (2016)

[6] J. Witek, S. Wang, B. Schroeder, R. Lingwood, A. Dounas, H.-J. Roth, M. Fouché, M. Blatter, O. Lemke, B. Keller, S. Riniker, Rationalization of the membrane permeability differences in a series of analogue cyclic decapeptides. J. Chem. Inf. Model. **59**, 294 (2019)

[7] S. Ono, M.R. Naylor, C.E. Townsend, C. Okumura, O. Okada, R.S. Lokey, Conformation and permeability: cyclic hexapeptide diastereomers. J. Chem. Inf. Model. **59**, 2952 (2019)

[8] R.M. Venable, A. Krämer, R.W. Pastor, Molecular dynamics simulations of membrane permeability. Chem. Rev. **119**, 5954 (2019)

[9] C.T. Lee, J. Comer, C. Herndon, N. Leung, A. Pavlova, R.V. Swift, C. Tung, C.N. Rowley, R.E. Amaro, C. Chipot, Y. Wang, J.C. Gumbart, Simulation-based approaches for determining membrane permeability of small compounds. J. Chem. Inf. Model. **56**, 721 (2016)

[10] R. Sun, Y. Han, J.M.J. Swanson, J.S. Tan, J.P. Rose, G.A. Voth, Molecular transport through membranes: accurate permeability coefficients from multidimensional potentials of mean force and local diffusion constants. J. Chem. Phys. **149**, 072310 (2018)

[11] M. Sugita, S. Sugiyama, T. Fujie, Y. Yoshikawa, K. Yanagisawa, M. Ohue, Y. Akiyama, Large-scale membrane permeability prediction of cyclic peptides crossing a lipid bilayer based on

enhanced sampling molecular dynamics simulations. J. Chem. Inf. Model. **61**, 3681 (2021)

[12] K. Moritsugu, K. Takeuchi, N. Kamiya, J. Higo, I. Yasumatsu, Y. Fukunishi, I. Fukuda, Flexibility and cell permeability of cyclic Ras-inhibitor peptides revealed by the coupled Nosé-Hoover equation. J. Chem. Inf. Model. **61**, 1921 (2021)

[13] R. Harada, R. Morita, Y. Shigeta, Free-energy profiles for membrane permeation of compounds calculated using rare-event sampling methods. J. Chem. Inf. Model. **63**, 259 (2023)

[14] S.M. Linker, C. Schellhaas, A.S. Kamenik, M.M. Veldhuizen, F. Waibl, H.J. Roth, M. Fouché, S. Rodde, S. Riniker, Lessons for oral bioavailability: how conformationally flexible cyclic peptides enter and cross lipid membranes. J. Med. Chem. **66**, 2773 (2023)

[15] S. Zhang, J.P. Thompson, J. Xia, A.T. Bogetti, F. York, A.G. Skillman, L.T. Chong, D.N. LeBard, Mechanistic insights into passive membrane permeability of drug-like molecules from a weighted ensemble of trajectories. J. Chem. Inf. Model. **62**, 1891 (2022)

[16] C.J. Dickson, V. Hornak, R.A. Pearlstein, J.S. Duca, Structure-kinetic relationships of passive membrane permeation from multiscale modeling. J. Am. Chem. Soc. **139**, 442 (2017)

[17] J.H. Prinz, H. Wu, M. Sarich, B. Keller, M. Senne, M. Held, J.D. Chodera, C. Schütte, F. Noé, Markov models of molecular kinetics: generation and validation. J. Chem. Phys. **134**, 174105 (2011)

[18] Z. Ghaemi, D. Alberga, P. Carloni, A. Laio, G. Lattanzi, Permeability coefficients of lipophilic compounds estimated by computer simulations. J. Chem. Theory Comput. **12**, 4093 (2016)

[19] M. Badaoui, A. Kells, C. Molteni, C.J. Dickson, V. Hornak, E. Rosta, Calculating kinetic rates and membrane permeability from biased simulations. J. Phys. Chem. B **122**, 11571 (2018)

[20] L.W. Votapka, R.E. Amaro, Multiscale estimation of binding kinetics using Brownian dynamics, molecular dynamics and milestoning. PLoS Comput. Biol. **11**, e1004381 (2015)

[21] N.G. van Kampen, *Stochastic Processes in Physics and Chemistry*, 3rd edn. (Elsevier, Amsterdam, 2007)

[22] D.T. Gillespie, A rigorous derivation of the chemical master equation. Physica A **188**, 404 (1992)

[23] B. Munsky, M. Khammash, The finite state projection algorithm for the solution of the chemical master equation. J. Chem. Phys. **124**, 044104 (2006)

[24] T. Jahnke, W. Huisinga, Solving the chemical master equation for monomolecular reaction systems analytically. J. Math. Biol. **54**, 1 (2007)

[25] R. Grima, P. Thomas, A.V. Straube, How accurate are the nonlinear chemical Fokker-Planck and chemical Langevin equations? J. Chem. Phys. **135**, 084103 (2011)

[26] D. Schnoerr, G. Sanguinetti, R. Grima, Approximation and inference methods for stochastic biochemical kinetics—a tutorial review. J. Phys. A: Math. Theor. **50**, 093001 (2017)

[27] A.V. Thomae, T. Koch, C. Panse, H. Wunderli-Allenspach, S.D. Krämer, Comparing the lipid membrane affinity and permeation of drug-like acids: the intriguing effects of cholesterol and charged lipids. Pharm. Res. **24**, 1457 (2007)

[28] G.A. Huber, S. Kim, Weighted-ensemble Brownian dynamics simulations for protein association reactions. Biophys. J. **70**, 97 (1996)

[29] D.M. Zuckerman, L.T. Chong, Weighted ensemble simulation: review of methodology, applications, and software. Annu. Rev. Biophys. **46**, 43 (2017)

[30] L.K. Buckton, M.N. Rahimi, S.R. McAlpine, Cyclic peptides as drugs for intracellular targets: the next frontier in peptide therapeutic development. Chem. Eur. J. **27**, 1487 (2021)

[31] M. Tanada, M. Tamiya, A. Matsuo, A. Chiyoda, K. Takano, T. Ito, M. Irie, T. Kotake, R. Takeyama, H. Kawada, R. Hayashi, S. Ishikawa, K. Nomura, N. Furuichi, Y. Morita, M. Kage, S. Hashimoto, K. Nii, H. Sase, K. Ohara, A. Ohta, S. Kuramoto, Y. Nishimura, H. Iikura, T. Shiraishi, Development of orally bioavailable peptides targeting an intracellular protein: from a hit to a clinical KRAS inhibitor. J. Am. Chem. Soc. **145**, 16610 (2023)

[32] D.J. Bicout, A. Szabo, Electron transfer reaction dynamics in non-Debye solvents. J. Chem. Phys. **109**, 2325 (1998)

[33] A. Furukawa, C.E. Townsend, J. Schwochert, C.R. Pye, M.A. Bednarek, R.S. Lokey, Passive membrane permeability in cyclic peptomer scaffolds is robust to extensive variation in side chain functionality and backbone geometry. J. Med. Chem. **59**, 9503 (2016)

[34] W.L. Jorgensen, J. Chandrasekhar, J.D. Madura, R.W. Impey, M.L. Klein, Comparison of simple potential functions for simulating liquid water. J. Chem. Phys. **79**, 926 (1983)

[35] S. Jo, T. Kim, V.G. Iyer, W. Im, CHARMM-GUI: A web-based graphical user interface for CHARMM. J. Comp. Chem. **29**, 1859 (2008); http://www.charmm-gui.org

[36] C.J. Dickson, B.D. Madej, Å.A. Skjevik, R.M. Betz, K. Teigen, I.R. Gould, R.C. Walker, Lipid14: the Amber lipid force field. J. Chem. Theory Comput. **10**, 865 (2014)

[37] B.D. Madej, I.R. Gould, R.C. Walker, A parameterization of cholesterol for mixed lipid bilayer simulation within the Amber Lipid14 force field. J. Phys. Chem. B **119**, 12424 (2015)

[38] J. Wang, R.M. Wolf, J.W. Caldwell, P.A. Kollman, D.A. Case, Development and testing of a general Amber force field. J. Comput. Chem. **25**, 1157 (2004)

[39] M.J. Frisch et al., Gaussian 16, Revision C.01 (Gaussian, Inc., Wallingford, 2016)

[40] K. Eyer, F. Paech, F. Schuler, P. Kuhn, R. Kissner, S. Belli, P.S. Dittrich, S.D. Krämer, A liposomal fluorescence assay to study permeation kinetics of drug-like weak bases across the lipid bilayer. J. Control. Release **173**, 102 (2014)

[41] D. Frezzato, Intrinsic timing in classical master equation dynamics from an extended quadratic format of the evolution law. J. Math. Chem. **61**, 806 (2023)

Supplementary Files

This is a list of supplementary files associated with this preprint. Click to download.

- SuplementMembraneMaster.pdf